CONF-780609--8

AN ANALYTICAL REPRESENTATION OF THE CREEP AND CREEP-RUPTURE BEHAVIOR OF ALLOY 800H*

M. K. Booker
Metals and Ceramics Division
Oak Ridge National Laboratory
Oak Ridge, Tennessee 37830

ABSTRACT

The extensive use of Alloy 800 (including the 800H variation) in elevated-temperature applications requires that the mechanical properties of this material be well characterized and understood. In the present investigation, available creep and creep-rupture data for Alloy 800H have been collected and analyzes. Results include mathematical models describing time and strain to rupture, time and strain to tertiary creep, and creep strain-time behavior as functions of stress and temperature.

*Research sponsored by the Department of Energy under contract with the Union Carbide Corporation.

EB

DISCLAIMER

An Analytical Representation of the Creep and Creep-Rupture Behavior of Alloy 800H

INTRODUCTION

The high nickel austenitic Alloy 800H is an important structural material for elevated-temperature nuclear vessels and components. In fact, it is one of only four materials currently approved under ASME Code Case 1592 [1] for nuclear service above 427°C (800°F). Many of the austenitic-to-ferritic transition weld joints [2] in the proposed Clinch River Breeder Reactor Plant (CRBRP) will consist of trimetallic joints employing a spool piece (about 30 cm long) of Alloy 800H between 2 1/4 Cr—1 Mo steel and austenitic stainless steel [3]. The use of a spool piece will reduce thermal stresses due to differences in the coefficients of expansion in the austenitic and ferritic piping materials. The transition joints will essentially consist of two welds: 2 1/4 Cr—1 Mo steel to Alloy 800H via ERNiCr—3 (Inconel 82) filler metal, and Alloy 800H to stainless steel via 16-812 filler metal. Successful design and inelastic analysis require that the behavior of these materials be well understood. Such an understanding requires, among other things, a thorough knowledge of the mechanical properties of the materials involved. Toward this end, a survey of available creep and tensile data for Alloy 800H has been completed. Many such data are available, but it is necessary to compile them and to present them in formats that are useful to designers. Therefore, the data have been analyzed to yield mathematical descriptions of the behavior of this important material.

BACKGROUND INFORMATION

The high nickel austenitic Alloys 800 and 800H have been used in a variety of applications including furnace equipment and reformer and cracker tubes for the petrochemical industry [4]. The relatively wide use of the material can be attributed to its excellent elevated-temperature strength and to its resistance to oxidation and carburization at high temperatures. Table I shows the

specifications on chemical composition currently used for Alloys 800 and 800H. In terms of chemistry, the only difference between the two is that Alloy 800H must have a minimum carbon content of 0.05 weight percent. Also, Alloy 800H is required to have a grain size of ASTM No. 5 or coarser. Finally, Alloy 800H is solution annealed at about 1150°C (2100°F), whereas Alloy 800 is mill-annealed at about 980°C (1800°F). (Before the advent of Alloy 800H, the material existed as a solution annealed "Grade 2" material and a mill-annealed "Grade 1" material.) The alloy is currently manufactured under a variety of trade names, including Incoloy 800, Escalloy 800, Carlson 800, Pyromet 800, Udimet 800, Sanicro 30 and 31, Croloy 20-30, Crucible 800, Camvac 800, and Hoskins Alloy 800 [5].

Alloy 800H is essentially a solid solution alloy, but its behavior can be strongly influenced by the precipitation of several phases within the material. These phases include gamma prime [$Ni_3(Al, Ti)$], chromium carbides ($Cr_{23}C_6$) and titanium carbonitrides [Ti(C,N)] [6]. Thus, it is to be expected that the concentrations of nickel, carbon, aluminum, titanium, and nitrogen may have significant influences upon the behavior of the material.

Much of the long-term elevated-temperature strength of Alloy 800H can in fact be attributed to the strengthening effects of precipitated phases. Unfortunately, these phases (particularly γ') may also cause decreases in the long-term ductility. Thus, it is important to examine trends in the creep ductility of the material.

Finally, the effects of precipitated phases can cause complications in the data analysis in two respects. First, the strengthening effects may be lost after long times due to overaging. Second, there is some evidence [7] that the effects of γ' precipitation on mechanical properties are small at about 700°C (1292°F) or above, but large in the range 500-650°C (632-1202°F). Unfortunately, most available U.S. creep data for Alloy 800H were obtained at temperatures of

649°C (1200°F) or above, while most CRBRP service will be from 538°C (1100°F). The problem of extrapolation of results from high to low temperatures is thus complicated by the metallurgy of the material.

DATA USED

All data used in this report were derived from tests on file in the ORNL Mechanical Properties Data Storage and Retrieval System (DSRS) [8]. The major original source of both creep and tensile data was the package [9] prepared by Huntington Alloys. Actual tensile stress-strain data for use in development of isochronous stress-strain curves were obtained privately from General Atomics Corporation [10]. Creep-strain-time curves from tests conducted by Huntington were obtained privately from C. E. Sessions and J. M. Duke of Westinghouse Tampa Division. Finally, due to the shortage of creep data, especially at low temperatures, data for Sanicro 31 from Sandvik Alloys [11] were examined. (Sanicro 31 is the Swedish solution annealed version of Alloy 800H.) Due to possible differences in alloy specifications and in testing techniques, the Sandvik data were not used in the final equation development. They are useful, however, in that they represent long-time data for many heats of material. Moreover, many data were obtained at temperatures of 550 and 600°C. All data used in equation development or for comparison purposed are tabulated in Ref. 12.

RESULTS

For CRBRP transition joint design, it is necessary to be able to predict the creep behavior of Alloy 800H from about 454°C (850°F) to 721°C (1350°F) [13] for both normal and off normal operating conditions. In order to encompass the complete service range, an analysis of data up to 760°C (1400°F) has been completed. For Alloy 800H data were available for temperatures below 649°C (1200°F), and none below 538°C (1000°F), but the results have been extrapolated down to 427°C (800°F). Properties examined include time and strain

to rupture, time and creep strain to tertiary creep, minimum creep rate, and creep strain-time behavior. Figure 1 defines the properties used, while Fig. 2 defines the conditions of available creep tests.

RUPTURE LIFE

The creep property that has received the most attention in the literature, and for which the most data are available, is the rupture life. In particular, the current analysis sought to obtain an equation expressing rupture life as a function of stress and temperature.

In the initial analyses of rupture life, data at temperatures up to 871°C (1600°F) were examined, but the results thusly obtained appeared biased toward the higher temperature data. In view of the complex precipitation phenomena mentioned above, it was decided to use only data up to 760°C since these data encompassed the desired temperature range and subsequent fits appeared more consistent with the lower temperature ($T \leq 649$°C) data.

The mathematical analysis of rupture data for a material such as Alloy 800H consists of two aspects. First, it is necessary to identify the effects of stress and temperature on the rupture life. Second, it is desirable to obtain an expression that will predict variations in the behavior of the material. Unfortunately, the current data base is not sufficient to clearly identify the effects of factors such as chemistry and grain size on the creep behavior. Previous results on types 304 and 316 stainless steel [14-17] and on 2 1/4 Cr-1 Mo steel [18] have shown that the elevated temperature ultimate tensile strength for material of a given heat and heat treatment can be an effective indicator of variations in creep strength, at least for test times up to and beyond 10,000 hrs. The current data for Alloy 800H, however, show little or no correlation between tensile strength and creep strength, as shown in Fig. 3. This lack of correlation may result from the precipitation effects on the creep strength that do not appeat in the brief time period involved in a tensile

test. A possible relationship between creep strength and the tensile strength of aged material is discussed below.

Thus, the 55 available experimental stress-rupture data were analyzed merely as functions of stress and temperature, using the regression techniques described in Ref. 12. Considering the large uncertainties involved, it was found that the data could be described by a simple Larson-Miller [19] parameter of the form

$$\log t_r = -18.45 + 3402/T - \frac{6430}{T} \log \sigma, \tag{1}$$

where t_r is the rupture life in hours, T is the temperature (K), and σ is the stress (MPa). Figure 4 compares the fit of Eq. 1 to the experimental data. Measuring the goodness of fit in terms of R^2, the coefficient of determination [17], the value was 88.4%. Thus, 88.4% of the variations in the data were described by the simple form of Eq. 1. More complicated models fit slightly better (R^2 for the best five term model was 90.9%) but this improvement was judged to be insignificant. The data do not warrant use of a more complicated model.

Define the standard error of estimate, SEE, as

$$SEE = \sqrt{\frac{\Sigma (y_i - \hat{y}_i)^2}{n-\nu}} \tag{2}$$

where the y_i are the experimental values of the dependent variable (here $\log t_r$), and the $\hat{y}_i$ are the corresponding values predicted by the model. The number of terms in the model is given by ν, while n is the number of data. It was found that the scatter band of behavior could be described by the value of $\log t_r$ predicted by Eq. 1 $\pm$ 2 SEE. Here, SEE was 0.272. Thus, the scatter in behavior about the mean t_r could be described approximately by a factor of 3.5 up or down. Figure 5 compares the available data with limits obtained in this way. It should

be emphasized that these limits are merely empirical descriptions of the width of the scatterband and that they have no real statistical meaning.

An apparent systematic deviation of the data from the predicted lines occurs in the data for Heat HH8808A at 649°C. Table II shows the chemical compositions of the heats of material used in this analysis. Heat HH8808A has a high combined Al and Ti content of 1.02%. Thus, it might be expected to be unusually strong at 649°C due to γ' precipitation.

Heat-to-heat variations in creep strength can be qualitatively examined by reference to some recent data from Huntington Alloys [6]. These data were generated on some experimental heats with the specific goal of examining the effects of chemistry and processing on the creep behavior of solution annealed Alloy 800 (not all heats meet the specifications for Alloy 800H). These heats were not used in the current analysis due to their experimental nature. Table III shows the chemical compositions of these heats.

An analysis of chemistry effects is beyond the scope of this report. Huntington [6] work has involved such an investigation, including a thermodynamic model for the precipitation of various phases and the subsequent effects on creep-rupture strength and ductility. They found the γ' phase to be the most potent strengthener, but that carbides and nitrides can also be important. More work is needed in this area, but the currently available results all appear consistent with the theory that γ' precipitation is important to the behavior of this material.

Another aspect of the data for the heats in Table III is that room temperature tensile data were obtained on aged as well as on as-annealed material. As shown in Fig. 6, there appears to be little correlation between room temperature tensile strength and 500-hour rupture strength at 649°C, even for heats specifically designed for the study of heat-to-heat variations. However, when the

tensile strengths are obtained on material aged 1000 hours at 649°C, there is a strong positive correlation between tensile strength and creep strength. Figure 7 shows that the effects of aging at 593°C are similar to those at 649°C. Figures 8 and 9 show that the correlation between aged tensile strength and creep strength begins to deteriorate at creep test temperatures of 704°C and above. For instance, at 760°C only three heats show unusually strong 500-hour creep strengths. These are Heat HF5982 with an extremely high Al content ahd Heats HG5985 and HG5986 with extremely high Ti contents. All results are again consistent with the explanation that precipitated phases (particularly γ') are the primary reason for heat-to-heat variability in this material.

A final source of information about the rupture behavior of annealed Alloy 800 is the extensive package of data prepared by Sandvik [11] for Sanicro 31. These data are especially relevant since they range from 550°C to 700°C with a significant number at 550 and 600°C. The package includes data for the effects of product form (bar or tube), chemistry, and solution treatment temperature. Detailed discussions of the Sandvik work can be found in Refs. 7, 20-23.

Our analysis of the Sandvik Canicro 31 data is described in detail elsewhere [12]. Interestingly, even when only data for material solution annealed at 1150°C that met the Alloy 800H chemistry specifications was considered, the Sandvik data showed consistently lower rupture strength (Fig. 10 and Table 4) than the Alloy 800H material discussed above.

A possible implication is that the data used in deriving Eq. 1 may well be representative of stronger than average heats of Alloy 800H. If this is the case, the predictions of Eq. 1 could be nonconservative. At present, Eq. 1 is recommended to describe the stress rupture behavior of this material. A further investigation of the differences between the Alloy 800H data and the Sanicro 31 data does appear to be warranted, however. The generation of more Alloy 800H at temperatures of 593°C and below should also be given priority attention.

TIME TO TERTIARY CREEP

Details of our analysis of data for time to tertiary creep are given in Ref. 12. Two measures of this time were examined. Denote the time to the first deviation from linear secondary creep as t_2; denote the 0.2% strain offset [24] time to tertiary creep as t_{ss}. Using methods similar to those discussed elsewhere [24], our results were as follows.

$$(593\text{-}760°C) \rightarrow t_{ss} = 0.000628 \exp (6108/T)\ t_r^{0.996} \quad (3)$$

$$(427\text{-}593°C) \rightarrow t_{ss} = 0.726\ t_r^{0.996} \quad (4)$$

$$(593\text{-}760°C) \rightarrow t_2 = 0.00135 \exp (54800/T)\ t_r^{0.940} \quad (5)$$

$$(427\text{-}593°C) \rightarrow t_2 = 0.759\ t_r^{0.940} \quad (6)$$

In Eqs. 3 and 5 T is the temperature (K). Figure 11 illustrates the fit of these equations to available data, while Table VII displays the predicted tertiary creep strengths in terms of t_{ss} (lower limit = average - 2SEE).

STRAIN TO RUPTURE

Since long-term ductility may be low in a precipitation-hardening material such as Alloy 800H, the available data for the total strain to creep-rupture were examined. This data set was roughly the same as that used above in the analysis of rupture life, including Sandvik Sanicro 31 data. As far as can be determined, all U.S. data were generated using specimen gauge lengths of approximately 2.54 cm (1 inch) and gauge diameters of 0.64 cm (0.25 inch). No specific information was available concerning the geometry of the Sanicro 31 specimens. Briefly, the results of the current analysis of the data for total elongation for creep-rupture can be summarized as follows [12]:

(1) The three Sanicro 31 data sets all yield similar results, and all predict greater ductility than the Alloy 800H data at 593°C and above.

The method used to analyze these data was similar to that proposed first by Smith [25], expanded by Goldhoff [26], and applied in detail by Booker, et al. [27]. Denoting the strain to rupture as e_t, the average strain rate to rupture $\dot{e}_t$, is defined by

$$\dot{e}_t = e_t/t_r. \tag{7}$$

Although the scatter in e_t is generally too great to permit a meaningful direct analysis such as used above for t_r and t_3, the quantity $\dot{e}_t$ often does permit such an analysis. Having estimates for $\dot{e}_t$ and t_r, one then simply multiplies these values to yield an estimate for e_t. Figure 12 illustrates the fits to data for $\dot{e}_t$, while the final results for e_t for the Alloy 800H data set was given by

$$\log e_t = 6.728 - 7218/T + \frac{982}{T} \log \sigma. \tag{8}$$

Figure 13 compares the predictions of these equations with the experimental data. Table 6 compares the predicted average and "minimum" values of e_t corresponding to rupture lives of 10^3 and 10^5 hrs for the various data sets examined [12]. Since the rupture lives are assumed, there is no error in t_r for these predictions. Thus, the minimum values of e_t were obtained simply by subtracting 2SEE for the various log $\dot{e}_t$ fits from the predicted values of log e_t.

(2) The scatter is large, but the predictions appear to adequately describe the trends apparent in the data. These trends include a tendency for ductility to increase as temperature increases and to decrease as the rupture life increases (stress and creep rate decrease).

(3) The low predicted values of e_t below about 593°C cannot be totally substantiated by existing data, but they appear consistent with the data that are available. These low values, together with the decrease in e_t as t_r increases

again indicate a need for more long time and low temperature test data for this material. Such data would permit a better quantitative estimate of any possible design problems due to a lack of creep ductility.

CREEP STRAIN TO TERTIARY CREEP

The amount of creep strain that a material can withstand can also be an important ductility criterion in elevated-temperature design [28]. Therefore, the available data for the creep strain to tertiary creep (corresponding to the above data for the time to tertiary creep) have been described as below, using techniques similar to those used for e_t. Details are given elsewhere [12], but the final results were

$$\log e_{ss} = 4.865 - 8360/T + \frac{1440}{T} \log \sigma \qquad (9)$$

and

$$\log e_2 = 7.238 - 11300/T + \frac{2150}{T} \log \sigma, \qquad (10)$$

where e_{ss} and e_2 are the creep strains corresponding to times of t_{ss} and t_2, respectively, (see Fig. 1). Figure 14 illustrates the fit to the data for e_2. Trends are somewhat similar to those seen above for e_t. At a given stress, e_2 increases with temperature; at a given temperature, e_2 increases with stress. At long times, e_2 can be quite small (e_2 = 0.2% in 10^5 hours at all temperatures).

CREEP STRAIN-TIME BEHAVIOR

For inelastic design analysis, it is necessary to be able to estimate the amount of creep strain that will be incurred by a material as a function of time, stress, and temperature. The current limited set of available creep curves for Alloy 800H make a precise analysis of such a complicated phenomenon quite difficult. However, it is possible to obtain estimates of creep strain-time behavior by making certain assumptions and approximations. A previous

analysis by Sterling [29] of creep strain-time behavior based on a power law strain-time form falls into this category. A new analysis will be used here to develop an alternative simplified equation, and the two equations will be compared with available experimental data.

While the Sterling approach is very simple, it does contain several disadvantages, which are detailed in Ref. 18. The analysis was done by fitting data for the time to 0.02, 0.05, 0.1, 0.15, 0.21 0.25, 0.3, 0.4, 0.5, 0.7, 1.0, and 2% creep strain. Whole creep curves were never fit. As a result, there is some question whether the predictions will yield creep curves whose shapes reflect the true shapes of the experimental creep curves. Our analyses have shown, in fact, that the experimental curve shapes are inconsistent with the power law form. Moreover, that form is intended for the description of primary creep only, whereas Sterling used it for primary and secondary creep. Garofalo [30] suggests the addition of a linear secondary term to make the equation applicable in that region.

The simplified nature of the Sterling apporach can be partially justified by the limited nature of the available creep data. However, our analyses showed that the individual experimental creep curves could be described much better by a rational polynomial creep equation. The many advantages of this equation form are discussed in Ref. 31. Also, such as in Refs. 14 and 15, the nature of this equation is such that its stress and temperature dependence can often be determined by very simplified methods.

As used here, the rational polynomial is given by

$$e_c = \frac{Cpt}{1 + pt} + \dot{e}_m t, \tag{11}$$

where e_c is the creep strain, t is the time, $\dot{e}_m$ is the minimum creep rate (%/hr), and C is the limiting value of the transient primary term. The parameter p is

related to the sharpness of the curvature of the primary creep region. From Eq. 11, the instantaneous creep rate $\dot{e}_c$ is given by

$$\dot{e}_c = \frac{Cp}{(1 + pt)^2} + \dot{e}_m, \tag{12}$$

and the initial creep rate $\dot{e}_o$ is given by

$$\dot{e}_o = Cp + \dot{e}_m. \tag{13}$$

Figure 15 summarizes the properties of the equation, while Refs. 14, 15, 18, 32, and 33 describe previous recent use of the equation for the analysis of creep data.

Our analysis of minimum creep rate data showed that $\dot{e}_m$ could be described by

$$\log \dot{e}_m = 28.84 - 46080/T + \frac{7610}{T} \log \sigma \tag{14}$$

with an R^2 value of 75.73%. The predictions of Eq. 14 are compared with the experimental data in Fig. 16.

From Fig. 15 it can easily be verified that the value of C (%) is approximately given by

$$C = e_2 = \dot{e}_m t_2 \tag{15}$$

where e_2 and t_2 are, as above, the strain (%) and the time (hr) to the onset of tertiary creep. Methods for the estimation of e_2, t_2, and $\dot{e}_m$ are given in previous sections of this report. These estimates can thus be used to derive a prediction for C.

Note that at any time t, we have

$$\frac{Cpt}{1 + pt} = FC, \tag{16}$$

where F is the fraction of the total C of the primary strain that has been exhausted (F = 0 at t = 0, F = 1 at t = ∞). Equation 16 can be arranged to yield

$$p = \frac{F/(1 - F)}{t} , \tag{17}$$

Next, we analyzed data for the time to the onset of secondary creep, t_1, resulting in an equation of the form

$$\log t_1 = -35.51 + 45300/T + 8.71 \log \sigma - \frac{12980}{T} \log \sigma. \tag{18}$$

Figure 17 illustrates the fit of Eq. 18 to the available data. Finally, we assumed that at $t = t_1$ F = 0.95, leading to

$$p = 19/t_1. \tag{19}$$

Comparison of this equation with experimental curves led to generally good results. Having estimates for C, p, and $\dot{e}_m$, the creep strain-time behavior of Alloy 800H can be predicted as a function of stress and temperature.

Comparisons of the predictions from this approach with available experimental creep curves and with the predictions of the Sterling equation are illustrated in Fig. 18. There is a great deal of uncertainty in the predictions, especially in the low temperature region, and some method of predicting strength variations would be desirable. For instance, Heat HH8808A creeps far less at 649°C than would be predicted. Still, the current results are generally acceptable for the available data, although the magnitude of predicted strain appears only slightly more accurate than that from the Sterling equation in most cases examined. The predictions from the Sterling equation are quite similar to those of the current equation in most cases. The main difference between the two is that the current

equation appears to depict more accurately the shapes of the individual creep curves. With the large uncertainties involved in the extrapolation of results, any advantage is welcome. The accuracies of the two equations can not, of course, be compared in the extrapolated region.

A convenient format to present the general predictions of a creep equation is through the use of isochronous stress-strain curves. These curves reflect total accumulated strain (creep strain and instantaneous strain) as a function of temperature and stress for given times. We have found that the tensile stress-strain behavior of Alloy 800H to 2.0% total strain can be represented by

$$\sigma - \sigma_0 = \frac{abe_p}{1 + be_p} + \dot{h}_m e_p \tag{20}$$

where σ is the stress (MPa) and e_p is the plastic strain (%). The remaining parameters are given by

$$\sigma_0 = 0.7\ \sigma_y \quad (\sigma_y = 0.2\%\ \text{offset yield strength}) \tag{21}$$

$$b = 40 \tag{22}$$

$$\dot{h}_m = 25.8 \tag{23}$$

$$\sigma_y\ (\text{MPa}) = 220.2 - 0.389T + 5.33 \times 10^{-4}T^2 - 2.58 \times 10^{-7}T^3 \tag{24}$$

and

$$a = \frac{9}{8}(\sigma_y - \sigma_0 - 0.2\dot{h}_m). \tag{25}$$

Equation 25 is based on the criterion that $e_p = 0.2\%$ where $\sigma = \sigma_y$.

Current isochronous stress-strain curves in Code Case 1592 [1] reflect somewhat higher estimated yield strengths than would be predicted by Eq. 24, and as a result the isochronous curves are somewhat higher [12]. Revised Code Case 1592 curves have recently been proposed [10] based on a lowering of the current code yield strengths and on the Sterling creep equation [29]. As illustrated in Figs. 19-21, these revised curves compare reasonably well with the curves predicted by the present creep and stress-strain equations.

LIMITATIONS

The above creep predictions are analytically valid under the following ranges of conditions:

Stress: 0 MPa < σ < ultimate tensile strength;

Temperature: 427°C (800°F) $\leq$ T $\leq$ 760°C (1400°F)

Time: 0 hr $\leq$ t $\leq$ time to tertiary creep.

It must be realized, however, that the actual validity of any equation beyond the range of existing data cannot be verified in the absence of a detailed physical theory for the subject process. No such theory exists for the creep of this material. In addition, whereas the current equations yield predictions for typical behavior, actual behavior can show wide variations. It is hoped that further studies can yield a quantitative understanding of these variations. Based on the currently available data, it is felt that the equations developed here yield a reasonable representation of the behavior of this material. However, as can be observed in Fig. 4, there are some indications that the predictions may not be accurate at low temperatures (T $\leq$ 593°C). Available data are not sufficient to verify this trend, and the current results indicate a strong need for additional low temperature data for this material.

SUMMARY

Available tensile and creep data for Alloy 800H have been collected and analyzed to yield analytical representations for the behavior of this important material. It is recognized that precipitation processes and other metallurgical phenomena play an important role in determining the behavior of this material. However, the current data base and the current understanding

of the metallurgy of Alloy 800H dictate that the analyses be empirical in nature. Specific results of the current study are listed below.

1. The 0.2% offset yield strength from monotonic tensile tests was expressed as a simple polynomial function of temperature.
2. The engineering stress-strain behavior to 2.0% total strain was expressed using the rational polynomial tensile equation,

$$\sigma - \sigma_0 = \frac{abe_p}{1 + e_p} + \dot{h}_m e_p \tag{20}$$

where σ is the stress and e_p is the plastic strain.

The remaining parameters are given by:

$$\sigma_0 = 0.7\ \sigma_y \text{ (0.2\% offset yield strength)}, \tag{21}$$

$$b = 40 \tag{22}$$

$$\dot{h}_m = 25.8 \tag{23}$$

and

$$a = \frac{9}{8}(\sigma_y - \sigma_0 - 0.2\ h_m). \tag{24}$$

Thus, the stress-strain behavior is given as a function of temperature and yield strength. Average, minimum, and maximum values of σ_y can be used to yield predicted stress-strain curves for average, minimum, and maximum strength material.

3. Several creep properties were expressed as simple functions of stress and temperature. These properties include time (t_r) and strain (e_t) to rupture, time and creep strain to tertiary creep (both 0.2% offset and first deviation from linearity), minimum creep rate ($\dot{e}_m$) and time to the onset of secondary creep (t_1). Although the available data are sparse (particularly at lower temperatures), the equations developed appear to describe the data well. There is a strong need for more low temperature data, however.

4. Rupture data for Sanicro 31 material indicate consistently lower strength and higher ductility than those for the Alloy 800H material, even when the Sanicro 31 material meets specifications for Alloy 800H. These differences need to be examined further.

5. The creep strain-time behavior of Alloy 800H was expressed using the rational polynomial creep equation,

$$e_c = \frac{Cpt}{1 + pt} + \dot{e}_m t \tag{11}$$

where e_c is the creep strain and t is the time. The parameter $\dot{e}_m$ is the minimum creep rate mentioned above. The remaining parameters are given by

$$C = e_2 - \dot{e}_m t_2 \tag{15}$$

where e_2 and t_2 are the time and strain to tertiary creep, while

$$p = 19/t_1, \text{ and} \tag{19}$$

$$\log \dot{e}_m = 28.84 - 46080/T + \frac{7610}{T} \log \sigma. \tag{14}$$

6. The predictions from the current creep equation are generally somewhat similar to those of the previously developed Sterling equation, although the current predicted curve shapes are more consistent with the shapes of available experimental creep curves. Predicted isochronous stress-strain curves compare reasonably well with those recently submitted to Code Case 1592.

7. Predicted behavior at temperatures of 593°C (1100°F) and below cannot be verified by experimental data. There is a serious shortage of low temperature creep data for this material.

REFERENCES

1. Interpretations of the ASME Boiler and Pressure Vessel Code, Case 1592, American Society of Mechanical Engineers, New York, 1974.
2. J. F. King, Behavior and Properties of Welded Transition Joints Between Austenitic Stainless Steels and Ferritic Steels - A Literature Review, ORNL-TM-5163 (November 1975).
3. R. L. Klueh and J. F. King, "Creep and Tensile Properties of Transition Weld Joint Materials," Mechanical Properties Test Data for Structural Materials Quarterly Progress Report, October 31, 1976, ORNL-5237, pp. 211-213.
4. S. J. Rosenberg, Nickel and Its Alloys, National Bureau of Standards Monograph 106, U.S. Department of Commerce, Washington, D.C., 1968, pp. 72-73.
5. R. T. King, et al., Report of Task Force on Alternate Structural Materials for Liquid Metal Fast Breeder Reactors, ORNL-5076 (May 1976), p. 108.
6. T. H. Bassford and D. W. Rahoi, "Effect of Composition and Processing on the Mechanical Properties of Incoloy Alloy 800 and Similar Ni-Fe-Cr Alloys," Metallurgy of Alloy 800 and Implication for Use in LMFBR Steam Generators, WTD-AMD-76-048, (Minutes of Meeting at Westinghouse Tampa Division, November 1976).
7. L. Egnell and N. G. Persson, "Creep-Rupture Ductility of Alloy 800," paper presented at the 18 ème Colloque de Métallurgie - Le Nickel et Son Rôle Spécifique Dans Certains Types D'Alliage - Saclay, June 23-25, 1975.
8. M. K. Booker and B. L. P. Booker, Development and Implementation of a Mechanical Properties Data Storage and Retrieval System, ORNL/TM-5330 (June 1976).

9. J. M. Martin, "Incoloy Alloy 800 Data for Use in Design of Gas Cooled and Liquid Metal Fast Reactors," Trip Report INCO/ORNL/RRD/WR&D/WTD Meeting on Development of an Advanced Material for Sodium Heated Steam Generators, January 17, 1975.

10. A. B. Smith, General Atomics Company, Private Communication, 1977.

11. L. Egnell and N. G. Persson, "Creep-Rupture Data for Sanicro 30/31," Data Package Privately Supplied to ORNL by Sandvik AB, Sandviken, Sweden.

12. M. K. Booker, V. B. Baylor, and B.L.P. Booker, *Survey of Available Creep and Tensile Data for Alloy 800H*, ORNL/TM-6029, to be published.

13. K. D. Challenger, General Electric Company, Fast Breeder Reactor Development, Private Communication, October 1975.

14. M. K. Booker and V. K. Sikka, *Analyses of the Creep Strain-Time Behavior of Type 304 Stainless Steel*, ORNL-5190 (October 1976).

15. M. K. Booker, *Mathematical Description of the Elevated-Temperature Creep Behavior of Type 304 Stainless Steel*, ORNL/TM-6110, to be published.

16. V. K. Sikka, M. K. Booker, and C. R. Brinkman, *Use of Ultimate Tensile Strength to Correlate and Predict Creep and Creep-Rupture Behavior of Types 304 and 316 Stainless Steel*, ORNL-5285 (October 1977).

17. M. K. Booker, "Regression Analysis of Creep-Rupture Data - A Practical Approach," report in preparation.

18. M. K. Booker, *Interim Analysis of the Creep Strain-Time Characteristics of Annealed and Isothermally Annealed 2 1/4 Cr-1 Mo Steel*, ORNL/TM-5831 (June 1977).

19. F. R. Larson and J. Miller, "A Time-Temperature Relationship for Rupture and Creep Stresses," *Trans. ASME*, Vol. 74, 1952, pp. 765-771.

20. L. Egnell, "Design Data," Paper No. 21, British Nuclear Energy Society Materials Conference - Status Review of Alloy 800, University of Reading, England, September 25-26, 1974.

21. N. G. Persson and L. Egnell, "Creep-Rupture Characteristics of Alloy 800 at Around 600°C," Sandvik AB, Sandviken, Sweden, unpublished document.

22. L. E. Svensson, G. L. Dunlop, and N. G. Persson, "Creep Fracture Modes in a Ti-Stabilized 20 Cr-30 Ni Austenitic Alloy," *Scandanavian Journal of Metallurgy*, Vol. 5, 1976, pp. 166-173.

23. A. Plumtree and N. G. Persson, "Influence of γ' Precipitation on the Creep Strength and Ductility of an Austenitic Fe-Ni-Cr Alloy," to be published in *Met. Trans.*

24. M. K. Booker and V. K. Sikka, Interrelationships Between Creep Life Criteria for Four Nuclear Structural Materials," *Nuc. Technology*, Vol. 30, July 1976, pp. 52-64.

25. G. V. Smith, Properties of Metals at Elevated Temperatures, McGraw-Hill, New York, 1950, p. 151.

26. R. M. Goldhoff, "A Method for Extrapolating Rupture Ductility," Elevated Temperature Testing Problem Areas, ASTM STP 488, American Society for Testing and Materials, Philadelphia, 1971, pp. 82-94.

27. M. K. Booker, C. R. Brinkman, and V. K. Sikka, Correlation and Extrapolation of Creep Ductility Data for Four Elevated-Temperature Structural Materials, MPC-1, ed., A. C. Schaefer, American Society of Mechanical Engineers, New York, 1975.

28. M. K. Booker and V. K. Sikka, *Predicting the Strain to Tertiary Creep for Elevated-Temperature Structural Materials*, ORNL/TM-5403, July 1976.

29. S. A. Sterling, *A Temperature-Dependent Power Law for Monotonic Creep*, GA-A13027 (Rev.), June 1974, Revised March 1976.

30. F. Garofalo, Fundamentals of Creep and Creep-Rupture in Metals, McMillan, New York, 1965, p. 16.

31. D. O. Hobson and M. K. Booker, *Materials Applications and Mathematical Properties of the Rational Polynomial Creep Equation*, ORNL-5202, December 1976.

32. W. E. Stillman, M. K. Booker, and V. K. Sikka, "Mathematical Description of the Creep Strain-Time Behavior of Type 316 Stainless Steel," Proceedings of the Second International Conference on Mechanical Behavior of Materials, Boston, August 16-20, 1976, pp. 424-428.

33. M. K. Booker, et al., "Mechanical Property Correlations for 2 1/4 Cr-1 Mo Steel in Support of Nuclear Reactor Systems Design," *Int. J. Pres. Ves. & Piping*, Vol. 5, No. 3, July 1977, pp. 181-205.

Table 1. Composition Specifications for Alloys 800 and 800H

Element	Content, wt %	
	Alloy 800[a] (Annealed at about 980°C)	Alloy 800H[b] (Annealed at about 1150°C)
C	0.10 max	0.05–0.10
Ti	0.15–0.60	0.15–0.60
Al	0.15–0.60	0.15–0.60
Ni	30–35	30–35
Cr	19–23	19–23
Si	1.0 max	1.0 max
Mn	1.5 max	1.5 max
Cu	0.75 max	0.75 max
S	0.015 max	0.015 max
Fe	Balance	Balance
Grain Size		ASTM No. 5 or coarser

[a]ASTM B 163.

[b]ASME Code Case 1592.

Table 2. Heats of Material Used in Analysis of the Creep Properties of Alloy 800H

Heat	Chemical Composition, wt %									
	C	Mn	Fe	S	Si	Cu	Ni	Cr	Al	Ti
HH8735A	0.04	0.55	45.28	0.007	0.41	0.41	31.31	21.29	0.29	0.39
HH8808A	0.05	0.83	45.15	0.009	0.42		31.06	21.46	0.51	0.51
HH7686A	0.07	0.97	45.88	0.007	0.47	0.38	30.94	21.26	0.39	0.49
HH3603A	0.06	1.03	46.42	0.007	0.41	0.30	31.33	20.42	0.39	0.46
HH8416A	0.10	0.88	45.31	0.007	0.29	0.44	31.99	20.96	0.48	0.37
HH8285A	0.08	0.80	45.55	0.007	0.37	0.40	32.20	20.75	0.50	0.41
HH7534A	0.06	0.98	45.70	0.007	0.42	0.33	31.35	21.13	0.43	0.52

Table 3. Experimental Heats Tested in Huntington Program

Heat	Chemical Composition, wt %										
	C	Mn	S	Si	Cu	Ni	Cr	Al	Ti	N	O
HF5978	0.057	0.90	0.004	0.44	0.52	33.09	22.16	0.29	0.39	0.021	0.060
HF5979	0.061	0.89	0.004	0.60	0.51	32.87	22.00	0.45	0.12	0.053	0.040
HF5980	0.062	0.90	0.004	0.47	0.50	33.15	22.51	0.73	0.51	0.036	0.030
HF5981	0.065	0.94	0.003	0.44	0.51	32.81	21.69	1.27	0.61	0.037	0.040
HF5982	0.063	0.94	0.004	0.47	0.52	32.74	21.80	1.61	0.70	0.027	0.020
HF5983	0.080	0.92	0.004	0.44	0.50	32.67	21.33	0.16	0.45	0.041	0.050
HF5984	0.070	0.95	0.003	0.49	0.50	32.76	21.79	0.22	0.87	0.020	0.050
HF5985	0.064	0.95	0.004	0.50	0.50	32.68	21.23	0.28	1.51	0.010	0.050
HF5986	0.066	0.94	0.003	0.49	0.51	32.91	21.86	0.31	1.82	0.014	0.040
HF5997	0.029	1.65	0.004	0.62	0.42	32.61	21.32	0.34	0.59	0.035	
HF5998	0.028	0.99	0.004	0.50	0.42	32.62	21.92	0.33	0.62	0.037	
HF5999	0.061	0.94	0.004	0.52	0.42	32.77	21.57	0.35	0.59	0.035	
HF6000	0.098	0.95	0.004	0.45	0.41	32.88	21.83	0.37	0.60	0.047	
HF6061	0.010	0.85	0.004	0.40	0.42	33.73	20.74	0.16	0.48	0.037	
HF6119	0.090	0.99	0.005	0.57	0.51	33.44	21.99	0.20	0.85	0.021	0.028
HF6134	0.007	0.87	0.005	0.47	0.37	33.14	21.68	0.27	0.64	0.012	0.023
HF6135	0.012	0.89	0.005	0.57	0.45	33.38	21.54	0.20	0.80	0.026	0.040
HV2968	0.020	0.91	0.003	0.57	0.29	32.87	20.71	0.11	0.20	0.019	
HV2969	0.020	0.91	0.004	0.61	0.31	32.59	21.62	0.56	0.64	0.016	0.020
HV2970	0.020	0.89	0.003	0.57	0.27	32.55	21.87	0.61	0.25	0.043	0.017
HV2771	0.020	0.90	0.003	0.60	0.33	32.37	21.76	0.20	0.60	0.037	0.017
HV2972	0.070	0.89	0.003	0.55	0.33	32.65	21.40	0.63	0.24	0.011	0.013
HV2973	0.080	0.89	0.003	0.62	0.34	32.24	21.97	0.22	0.64	0.008	0.017
HV2974	0.080	0.87	0.003	0.54	0.27	32.62	21.80	0.20	0.22	0.040	0.016
HV2975	0.070	0.90	0.003	0.59	0.32	32.56	21.66	0.64	0.64	0.039	0.018
HV3105	0.017	0.99	0.003	0.63	0.48	32.82	20.74	0.40	0.41	0.016	0.016
HV3106	0.050	0.89	0.002	0.71	0.46	32.42	21.26	0.11	0.64	0.018	0.037
HV3107	0.130	0.91	0.002	0.66	0.51	32.07	21.46	0.13	0.27	0.014	0.023
HV3108	0.130	0.89	0.003	0.66	0.53	32.19	21.07	0.57	0.69	0.013	0.039
HV3114	0.050	0.87	0.003	0.58	0.51	32.57	21.39	0.01	0.53	0.012	0.034
HV3115	0.090	0.88	0.003	0.60	0.52	32.14	20.78	0.01	0.61	0.014	0.031
HV3185	0.020	0.93	0.005	0.64	0.33	35.07	20.40	0.03	0.60	0.007	0.035

Table 4. Estimated Rupture Strengths for the Various Rupture Life Data Sets Examined

Temperature		10^3-hr Rupture Strength, MPa (ksi)		10^5-hr Rupture Strength, MPa (ksi)	
(°C)	(°F)	Average	Lower Limit[a]	Average	Lower Limit[a]
		Alloy 800H[b]			
427	800	903 (131)	788 (114)	547 (79.3)	478 (69.2)
482	900	592 (85.9)	511 (74.2)	345 (50.0)	298 (43.2)
538	1000	385 (55.8)	329 (47.7)	215 (31.2)	184 (26.7)
593	1100	252 (36.6)	213 (30.9)	136 (19.7)	115 (16.6)
649	1200	164 (23.8)	137 (19.9)	85 (12.3)	71 (10.3)
704	1300	108 (15.6)	69 (12.9)	53 (7.8)	44 (6.4)
760	1400	70 (10.2)	57 (8.5)	33 (4.8)	27 (4.0)
		Sanicro 31 Complete Data Set[c]			
427	800	1120 (162)	866 (126)	509 (73.8)	393 (57.0)
482	900	597 (86.6)	462 (67.0)	271 (39.3)	210 (30.4)
538	1000	344 (49.9)	266 (38.6)	156 (22.6)	121 (17.5)
593	1100	214 (31.0)	166 (24.1)	97 (14.1)	75 (10.9)
649	1200	140 (20.3)	108 (15.7)	64 (9.2)	49 (7.1)
704	1300	97 (14.1)	75 (10.9)	44 (6.4)	34 (4.9)
760	1400	69 (10.1)	54 (7.8)	32 (4.6)	24 (3.5)
		Sanicro 31 1150°C Solution Annealed[d]			
427	800	1217 (176)	964 (140)	567 (82.2)	450 (65.3)
482	900	637 (92.4)	505 (73.2)	297 (43.1)	235 (34.1)
538	1000	361 (52.4)	286 (41.5)	168 (24.4)	133 (19.3)
593	1100	222 (32.2)	176 (25.5)	103 (14.9)	82 (11.9)
649	1200	143 (20.7)	114 (16.5)	67 (9.7)	53 (7.7)
704	1300	98 (14.2)	78 (11.3)	46 (6.6)	36 (5.2)
760	1400	70 (10.1)	55 (8.0)	32 (4.7)	26 (3.7)
		Sanicro 31 1150°C Solution Annealed Meeting Alloy 800H Specifications[e]			
427	800	1223 (177)	1010 (146)	559 (81.1)	462 (67.0)
482	900	642 (93.1)	530 (76.9)	293 (42.5)	242 (35.1)
538	1000	364 (52.8)	301 (43.6)	166 (24.1)	137 (19.9)
593	1100	224 (32.5)	185 (26.8)	102 (14.8)	85 (12.3)
649	1200	145 (21.0)	120 (17.4)	66 (9.6)	55 (8.0)
704	1300	99 (14.4)	82 (11.9)	45 (6.6)	38 (5.4)
760	1400	70 (10.2)	58 (8.4)	32 (4.7)	27 (3.9)

[a] Estimate from log t_r − 2SEE lower limits.

[b] Predictions from Eq. (11).

[c] Predictions from Eq. (13).

[d] Predictions from Eq. (14).

[e] Predictions from Eq. (15).

Table 5. Estimated Tertiary Creep Strength for Alloy 800H (0.2% Offset)

Temperature		10^3-hr Tertiary Creep Strength, MPa (ksi)		10^5-hr Tertiary Creep Strength, MPa (ksi)	
(°C)	(°F)	Average	Lower Limit	Average	Lower Limit
427	800	870 (126)	697 (101)	526 (76.2)	421 (61.1)
482	900	568 (82.4)	448 (64.9)	330 (47.9)	260 (37.7)
538	1000	368 (53.4)	285 (41.4)	206 (29.8)	159 (23.1)
593	1100	241 (34.9)	183 (26.6)	129 (18.7)	98 (14.2)
649	1200	147 (21.3)	110 (15.9)	76 (11.0)	57 (8.2)
704	1300	90 (13.1)	66 (9.6)	45 (6.5)	33 (4.8)
760	1400	55 (8.0)	40 (5.8)	26 (3.8)	19 (2.7)

Table 6. Estimated Values of Total Elongation to Creep Rupture for the Various Data Sets Examined.

TEMPERATURE °C (°F)	10^3 hr RUPTURE ELONGATION (%)		10^5 hr RUPTURE ELONGATION (%)	
	AVERAGE	LOWER LIMIT	AVERAGE	LOWER LIMIT
		Alloy 800H		
427 (800)	3.6	0.4	1.8	0.2
482 (900)	5.9	0.7	2.9	0.4
538 (1000)	9.1	1.1	4.5	0.6
593 (1100)	13.1	1.6	6.5	0.8
649 (1200)	18.1	2.2	9.0	1.1
704 (1300)	24.2	3.4	11.8	1.4
760 (1400)	31.2	3.8	15.3	1.9
		Sanicro 31 Complete Data Set		
427 (800)	7.5	0.6	4.4	0.4
482 (900)	11.7	1.0	6.8	0.6
538 (1000)	17.3	1.4	10.1	0.8
593 (1100)	24.1	2.0	14.0	1.2
649 (1200)	32.4	2.7	19.0	1.6
704 (1300)	42.0	3.5	24.5	2.0
760 (1400)	53.0	4.4	31.3	2.6
		Sanicro 31 1150°C Solution Annealed		
427 (800)	4.2	0.4	2.6	0.2
482 (900)	7.5	0.7	4.8	0.5
538 (1000)	12.5	1.2	8.0	0.8
593 (1100)	19.4	1.9	12.3	1.2
649 (1200)	28.8	2.8	18.3	1.8
704 (1300)	40.6	3.9	25.9	2.5
760 (1400)	55.7	5.4	35.0	3.4
		Sanicro 31 1150°C Solution Annealed Meeting Alloy 800H Specifications		
427 (800)	7.5	1.3	3.8	0.6
482 (900)	11.5	1.9	5.9	1.0
538 (1000)	16.6	2.8	8.5	1.4
593 (1100)	22.8	3.8	11.6	2.0
649 (1200)	30.3	5.1	15.4	2.6
704 (1300)	38.7	6.5	19.7	3.3
760 (1400)	48.4	8.2	24.7	4.2

FIGURES

12. Comparison between experimental average strain rate to rupture data for Alloy 800H and predicted behavior.

13. Comparison between experimental and predicted values of total elongation to creep rupture for Alloy 800H.

14. Predicted and experimental values of the creep strain to tertiary creep (no offset) for Alloy 800H.

15. Schematic illustration of the properties of the rational polynomial creep equation.

16. Comparison between predicted and experimental data for minimum creep rate for Alloy 800H.

17. Comparison between experimental and predicted values of the time to the onset of secondary creep for Alloy 800H.

18. Comparison of predicted creep strain-time behavior with experimental data. Solid lines predicted from the current equation. Dashed lines predicted from the Sterling equation. (a) Heat HH8735A, 345 MPa, 538°C; (b) Heat HH8735A, 207 MPa, 593°C; (c) Heat HH7686A, 103 MPa, 649°C; (d) Heat HH7686A, 55 MPa, 704°C; (e) Heat HH8808A, 55 MPa, 760°C.

19. Comparison of isochronous stress-strain curves at 538°C (1000°F) predicted from the current equations with curves recently proposed for entry in Code Case 1592.

20. Comparison of isochronous stress-strain curves at 649°C (1200°F) predicted from the current equations with curves recently proposed for entry in Code Case 1592.

21. Comparison of isochronous stress-strain curves at 760°C (1400°F) predicted from the current equations with curves recently proposed for entry in Code Case 1592.

1. Definition of the creep properties examined in this report.

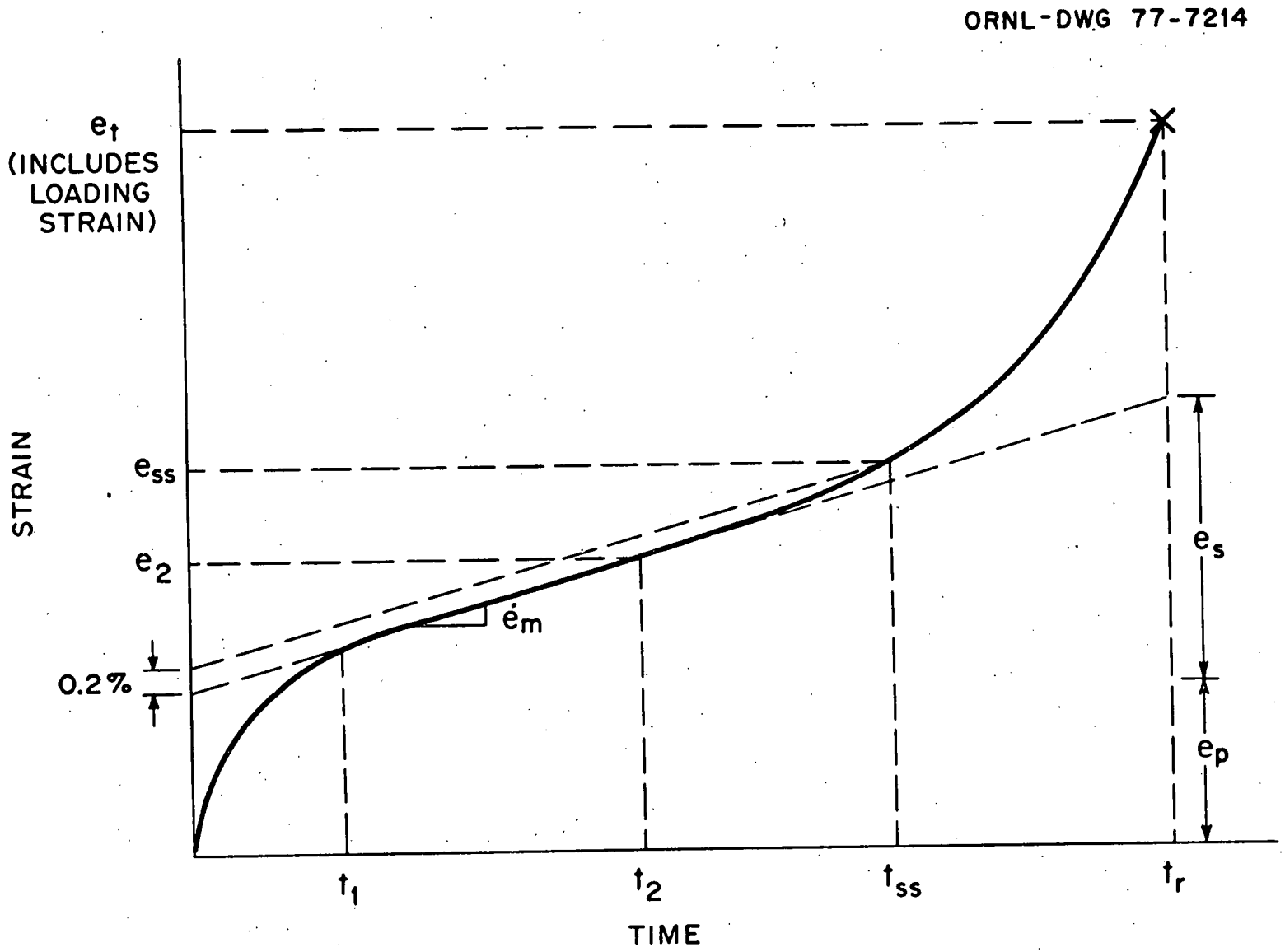

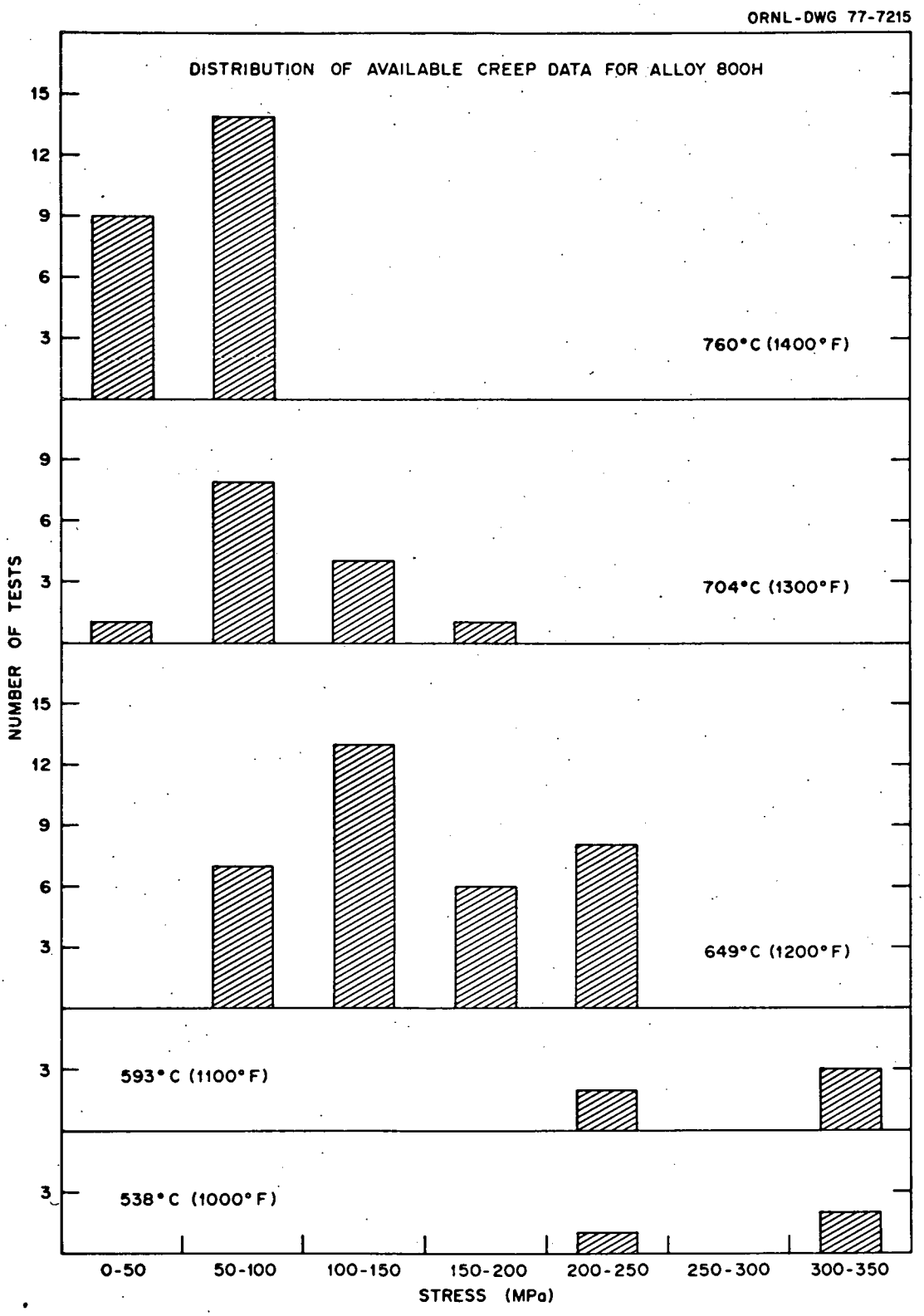

2. Frequency diagram of available creep tests for Alloy 800H in terms of stress and temperature.

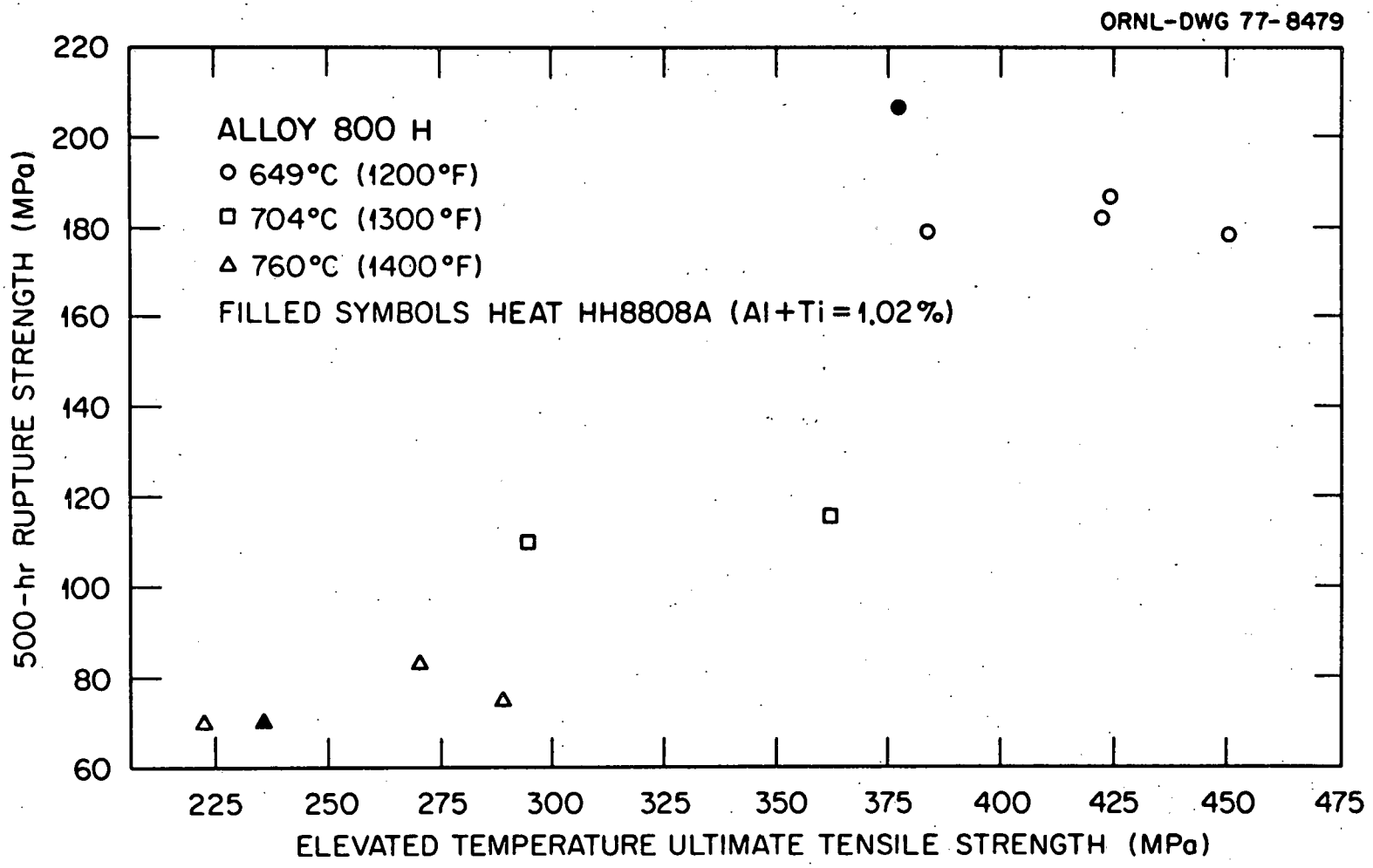

3. Relationship between ultimate tensile strength and 500-hour creep rupture strength for Alloy 800H.

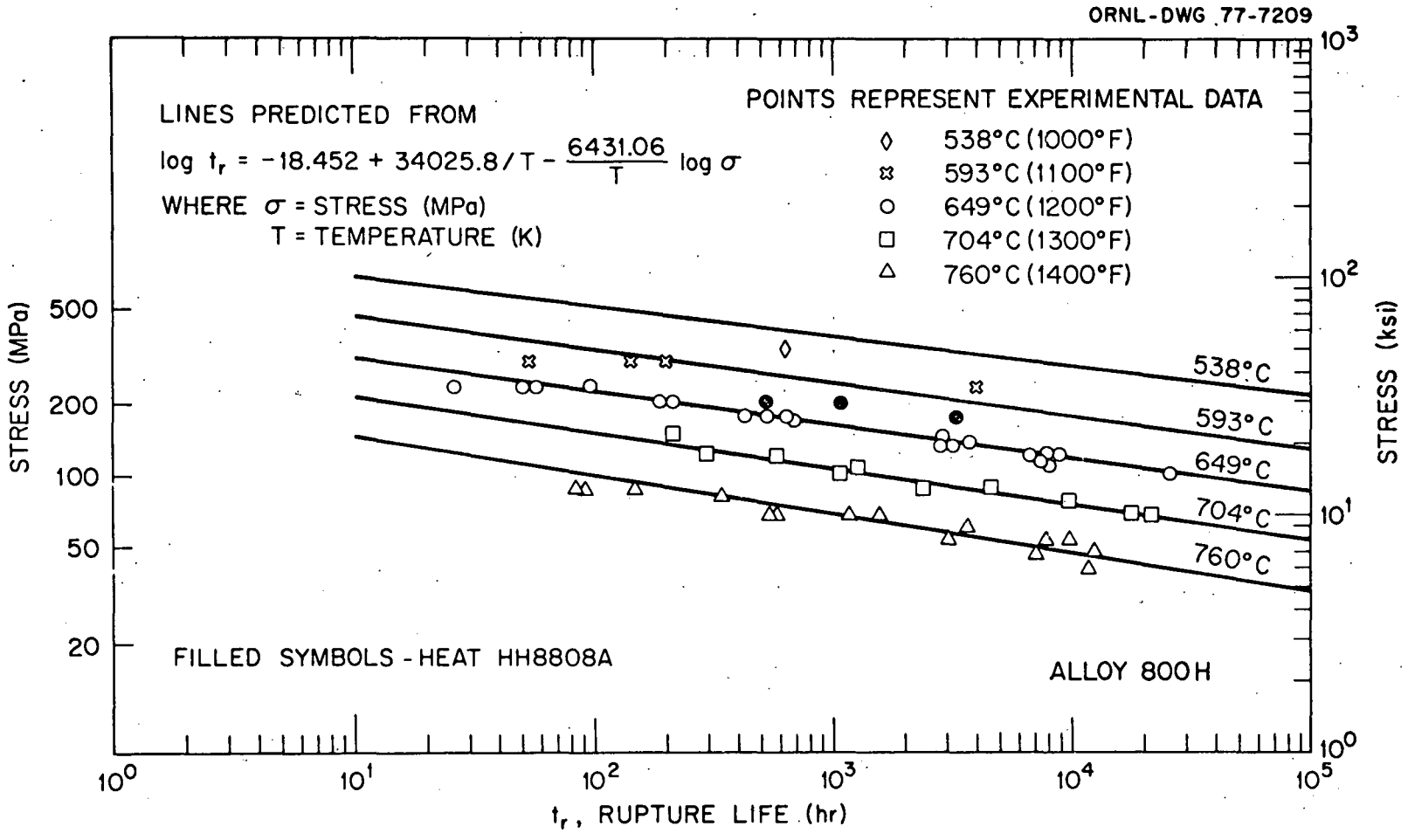

4. Comparison of experimental stress rupture data with predicted behavior for Alloy 800H.

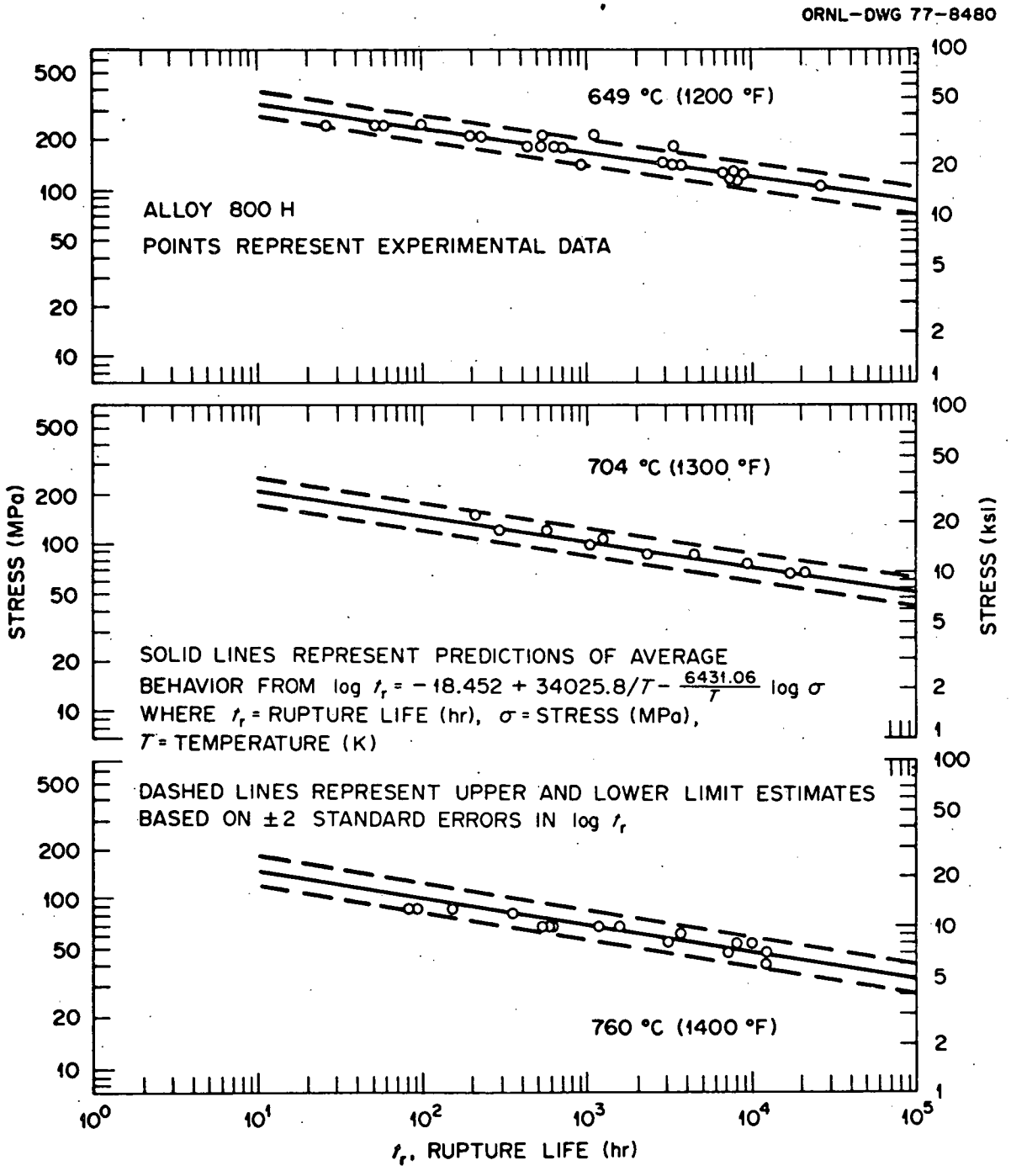

5. Comparison of experimental data with predicted mean behavior and ± 2SEE upper and lower limit behavior for Alloy 800H.

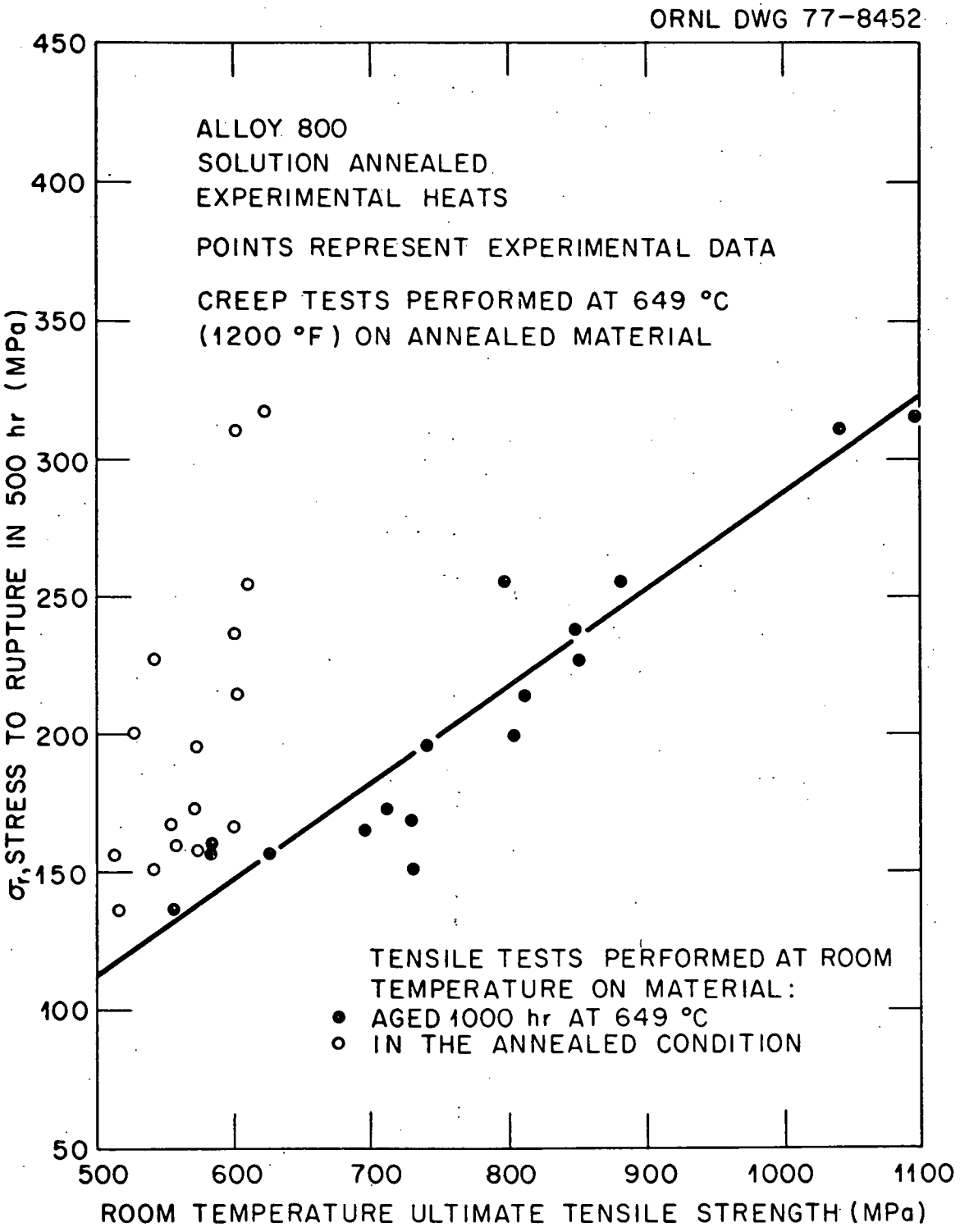

6. Relationship between room temperature ultimate tensile strength of solution annealed and of aged Alloy 800 and the 500-hour creep rupture strength of solution annealed Alloy 800 at 649°C (1200°F).

7. Relationship between room temperature utlimate tensile strength of Alloy 800 aged at 593°C (1100°F) or 649°C (1200°F) and the 500-hour creep rupture strength of solution annealed Alloy 800 at 593°C (1100°F).

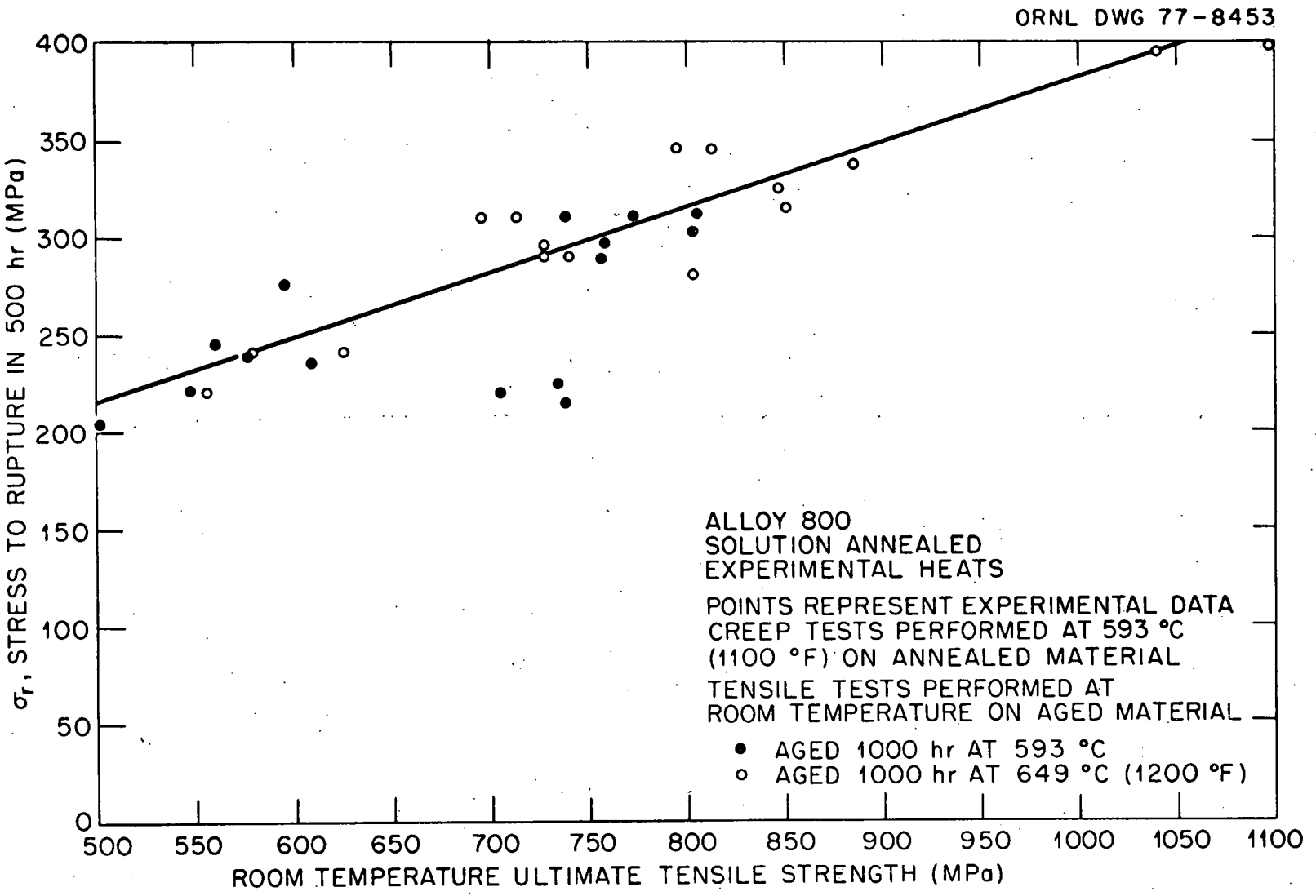

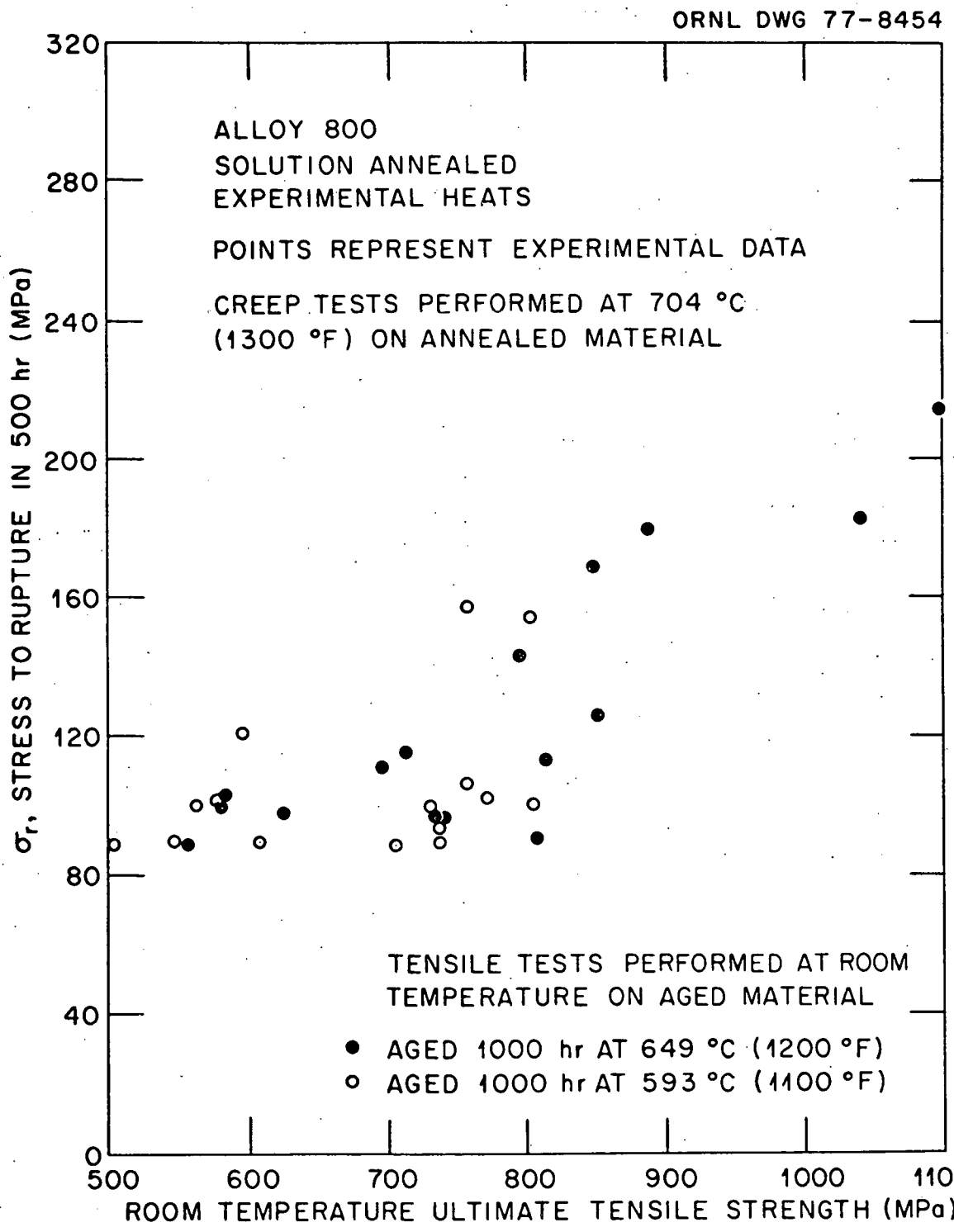

8. Relationship between room temperature ultimate tensile strength of Alloy 800 aged at 593°C (1100°F) or 649°C (1200°F) and the 500-hour creep rupture strength of solution annealed Alloy 800 at 704°C (1300°F).

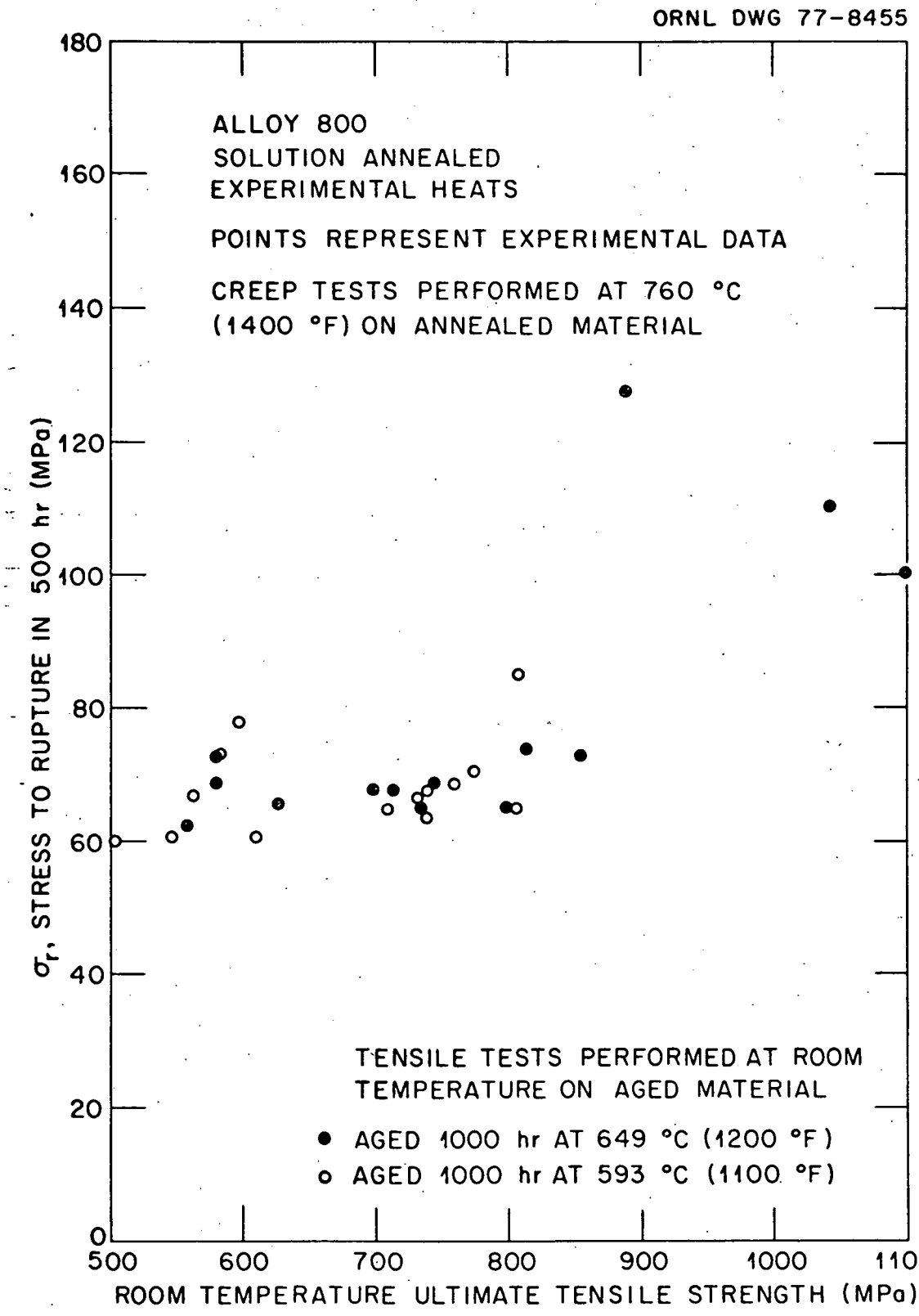

9. Relationship between room temperature ultimate tensile strength of Alloy 800 aged at 593°C (1100°F) or 649°C (1200°F) and the 500-hour creep rupture strength of solution annealed Alloy 800 at 760°C (1400°F).

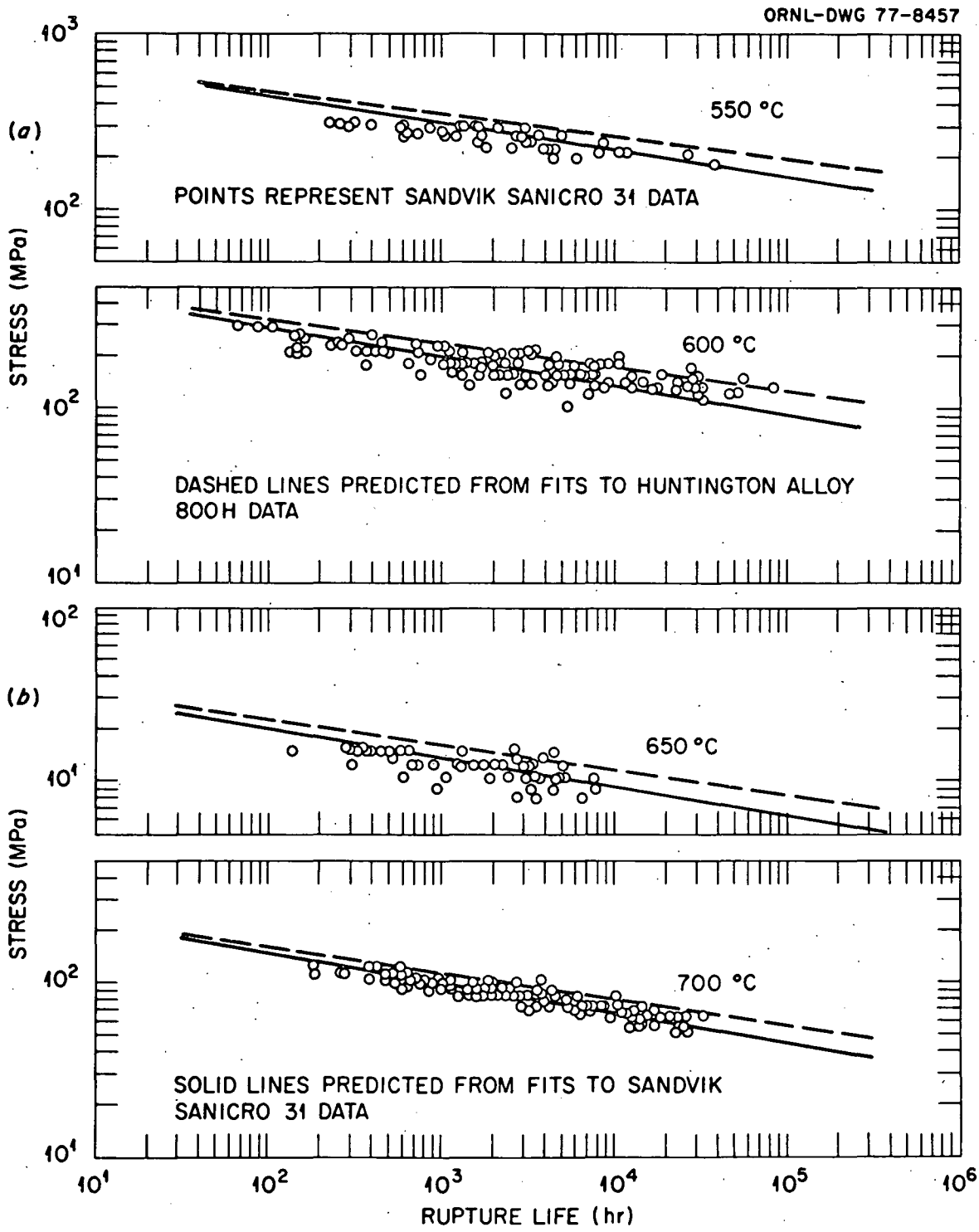

10. Comparison among the experimental Sandvik Sanicro 31 stress-rupture data and the predicted behavior based on these data and on the Huntington data for Alloy 800H.

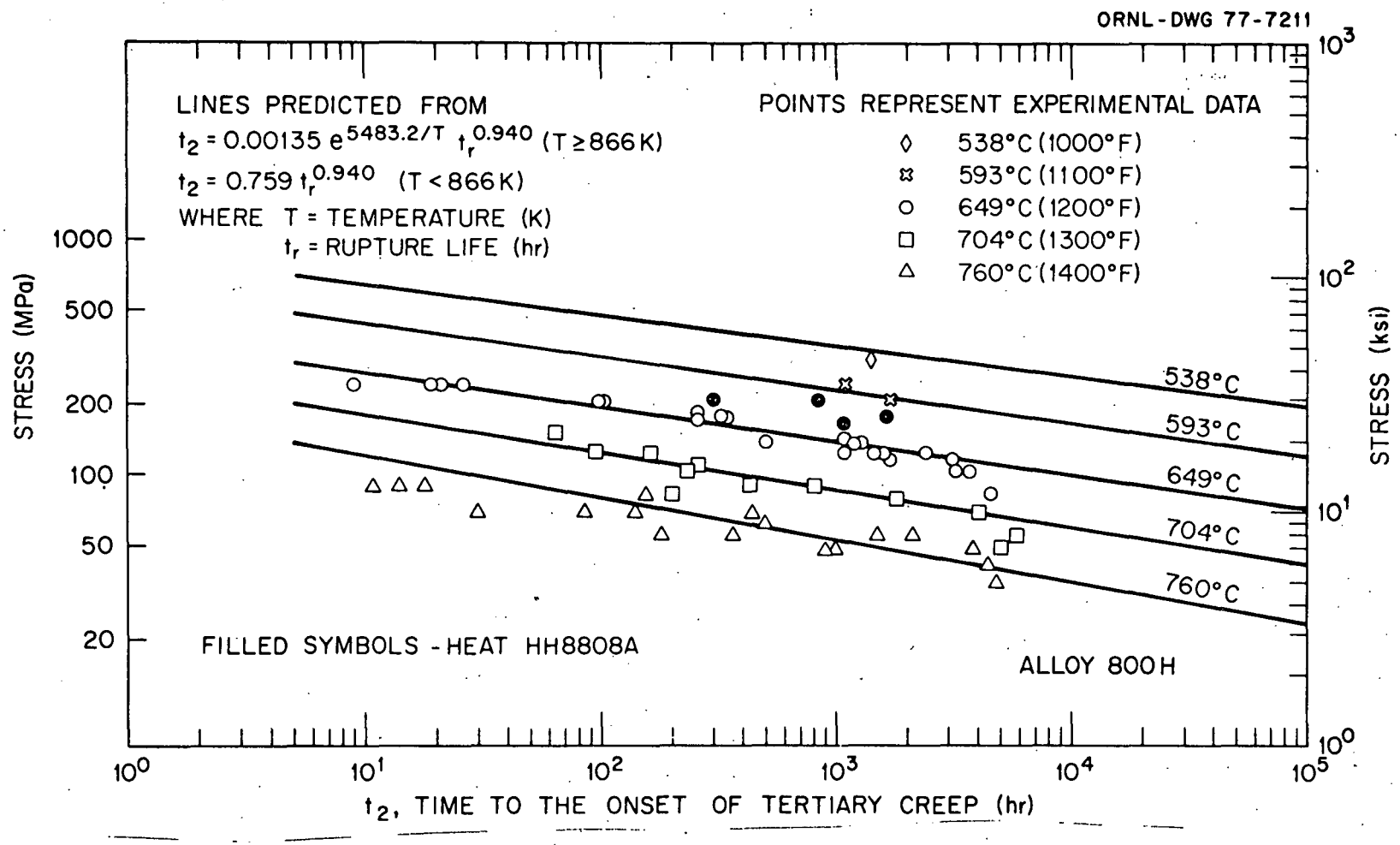

11. Comparison between experimental time to tertiary creep (no offset) data for Alloy 800H and predicted behavior from the recommended temperature-dependent relationship between rupture life and time to tertiary creep.

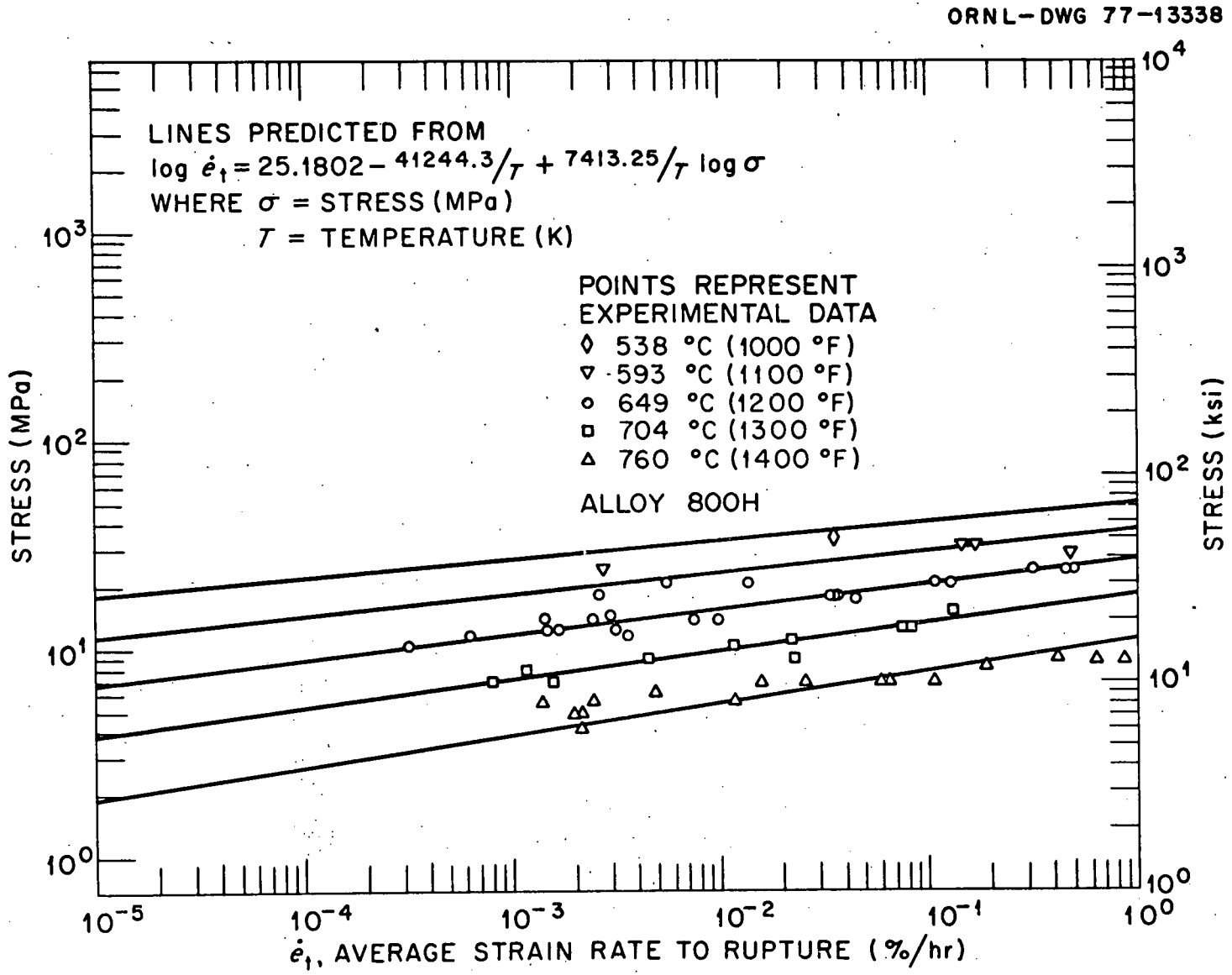

12. Comparison between experimental average strain rate to rupture data for Alloy 800H and predicted behavior.

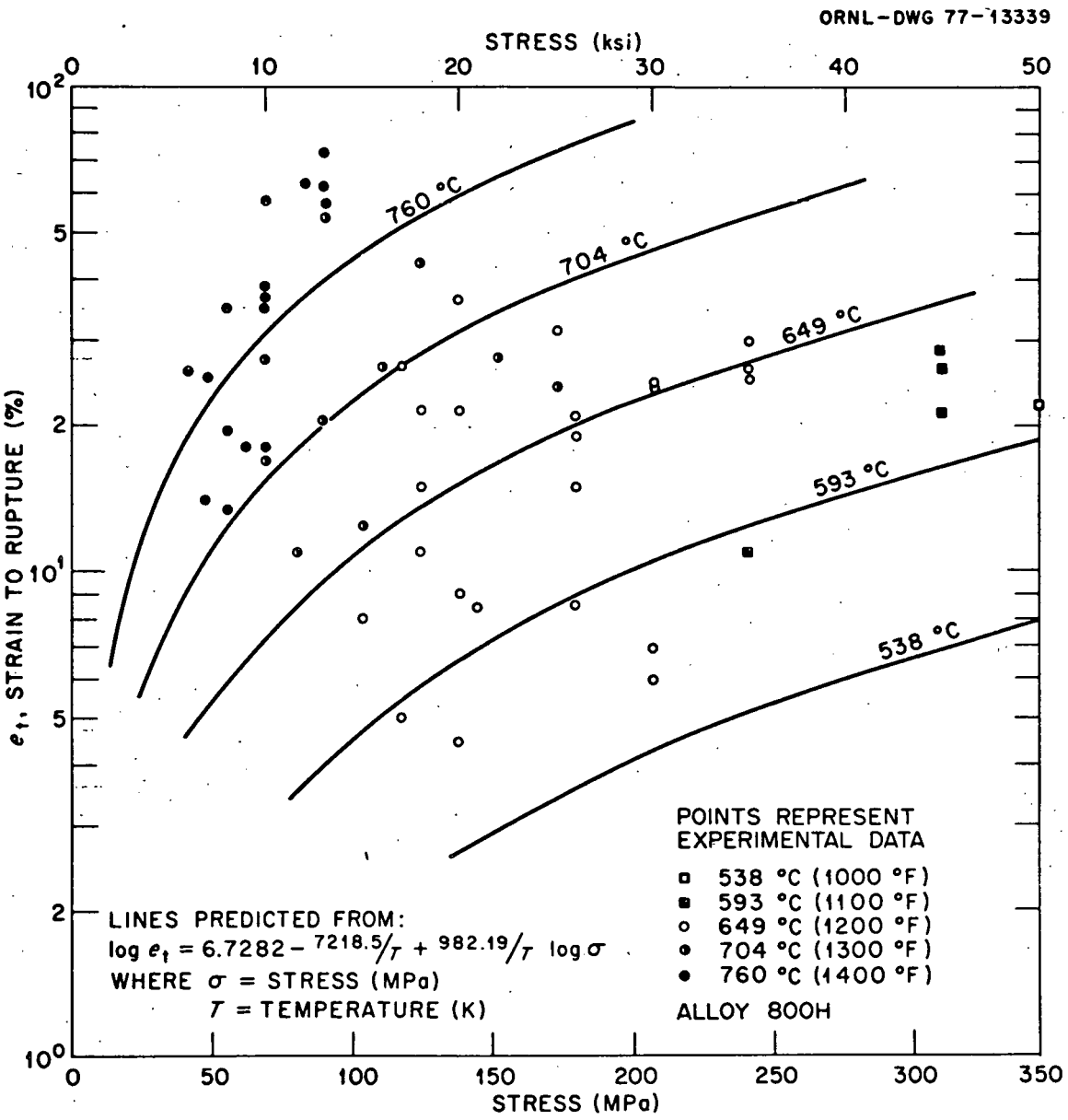

15. Comparison between experimental and predicted values of total elongation to creep rupture for Alloy 800H.

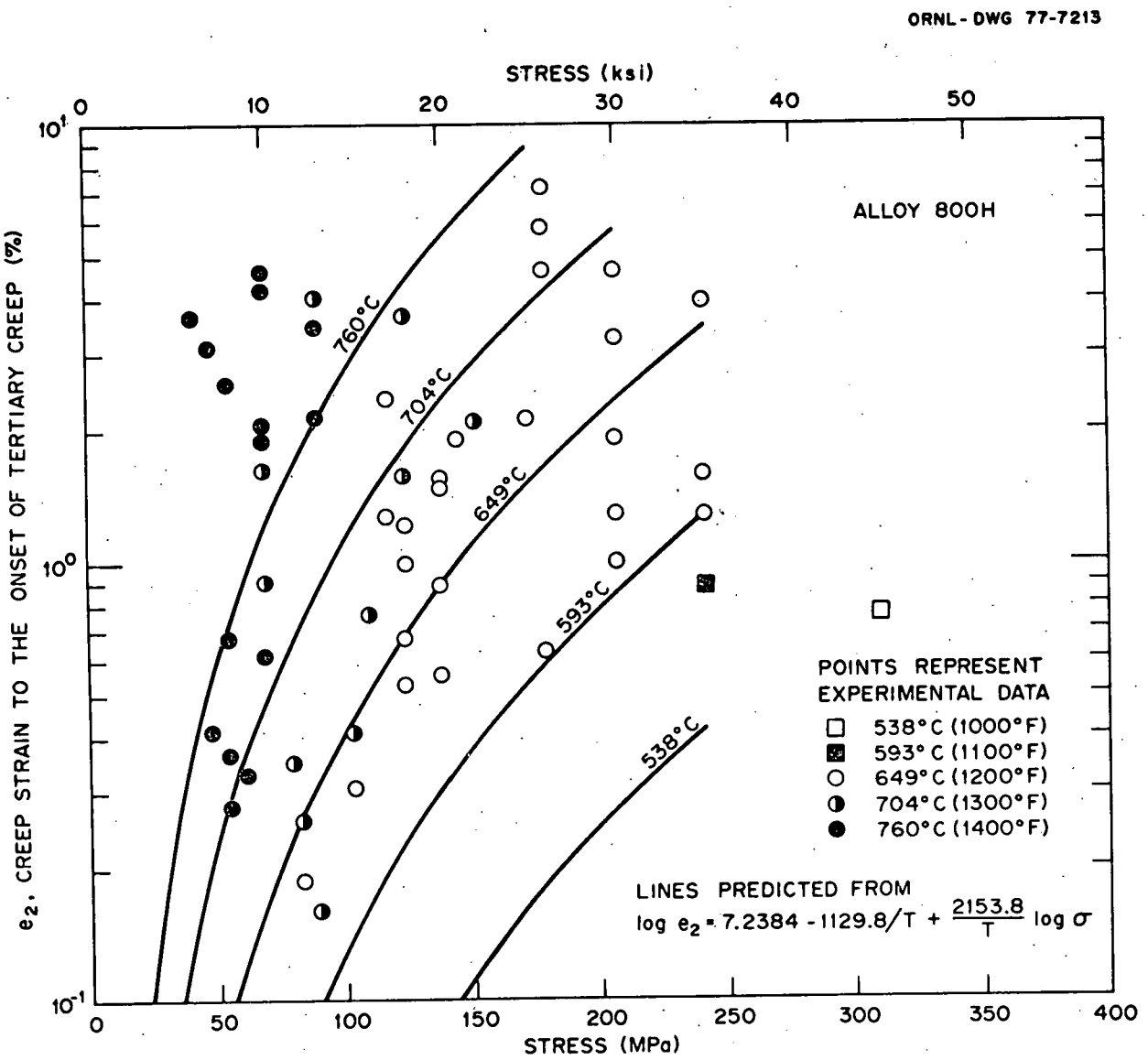

14. Predicted and experimental values of the creep strain to tertiary creep (no offset) for Alloy 800H.

ORNL-DWG 76-3985R

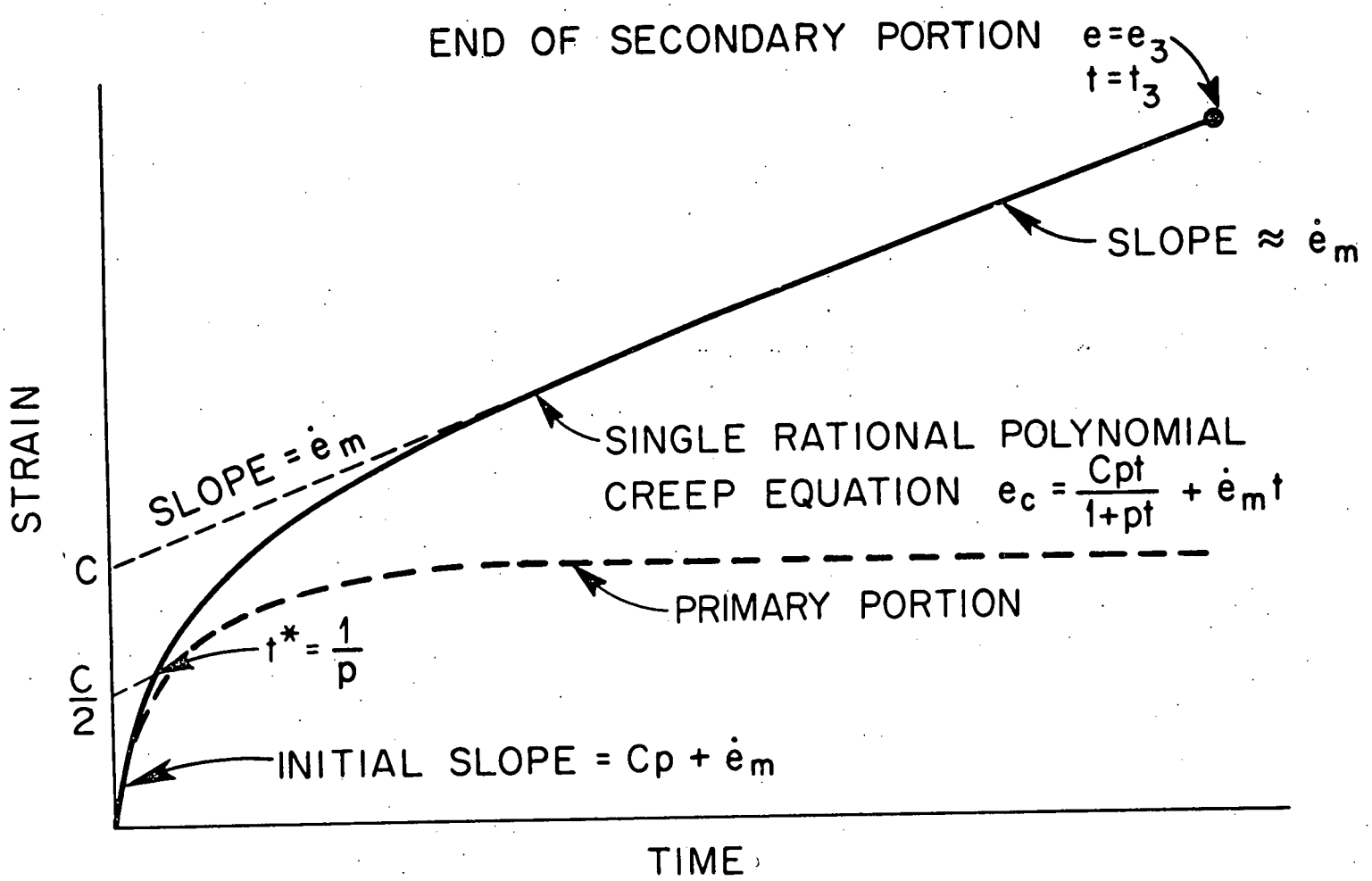

15. Schematic illustration of the properties of the rational polynomial creep equation.

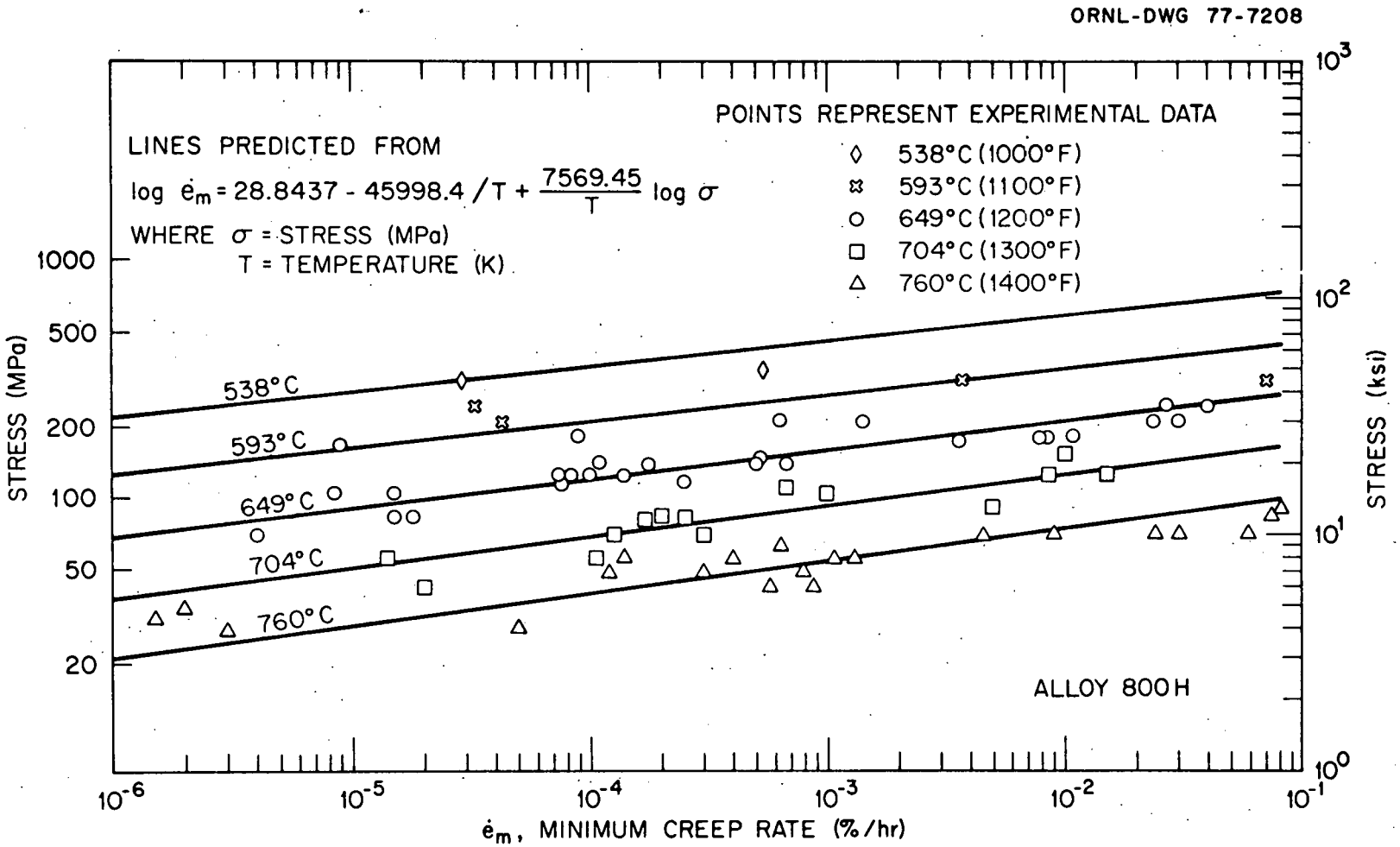

16. Comparison between predicted and experimental data for minimum creep rate for Alloy 800H.

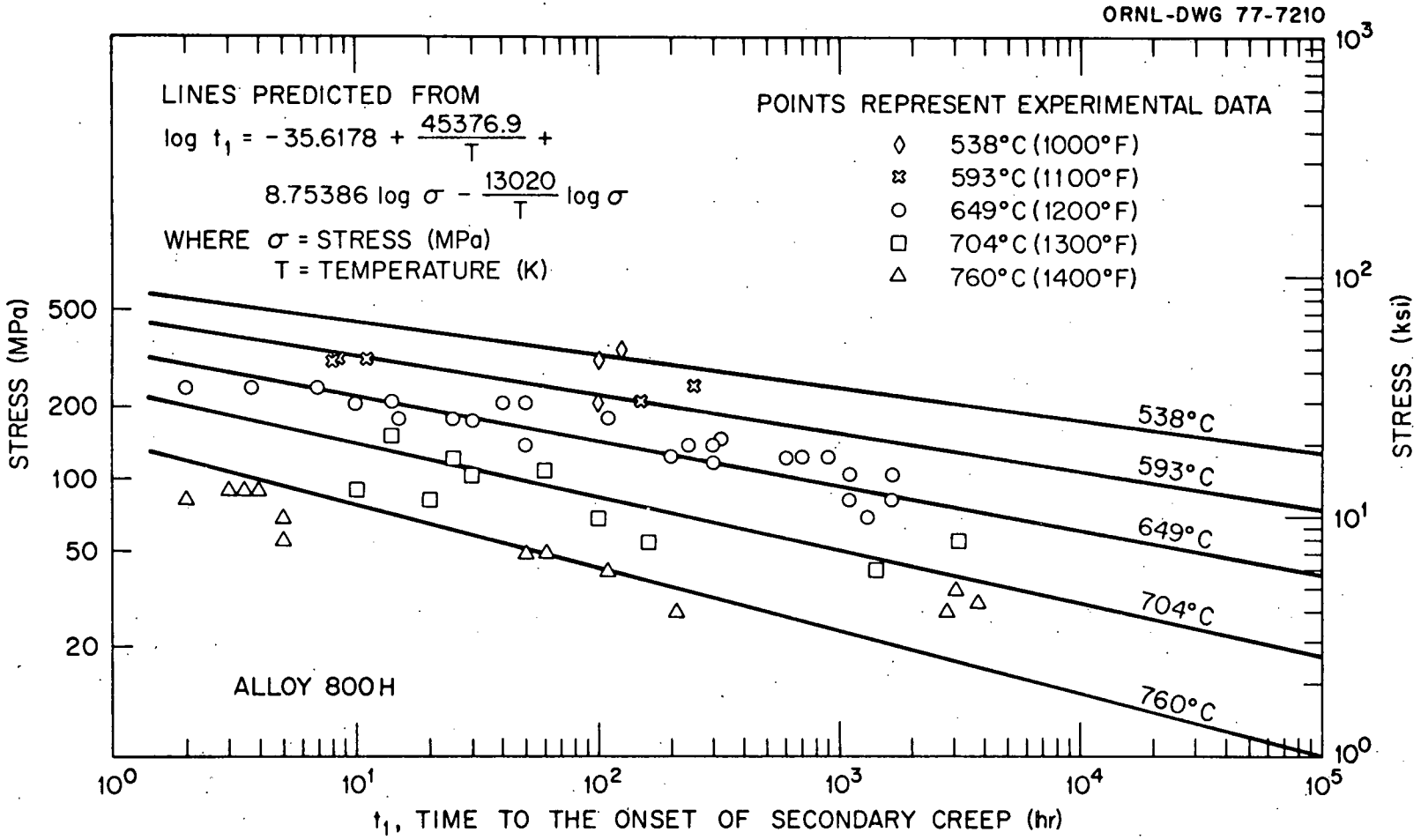

17. Comparison between experimental and predicted values of the time to the onset of secondary creep for Alloy 800H.

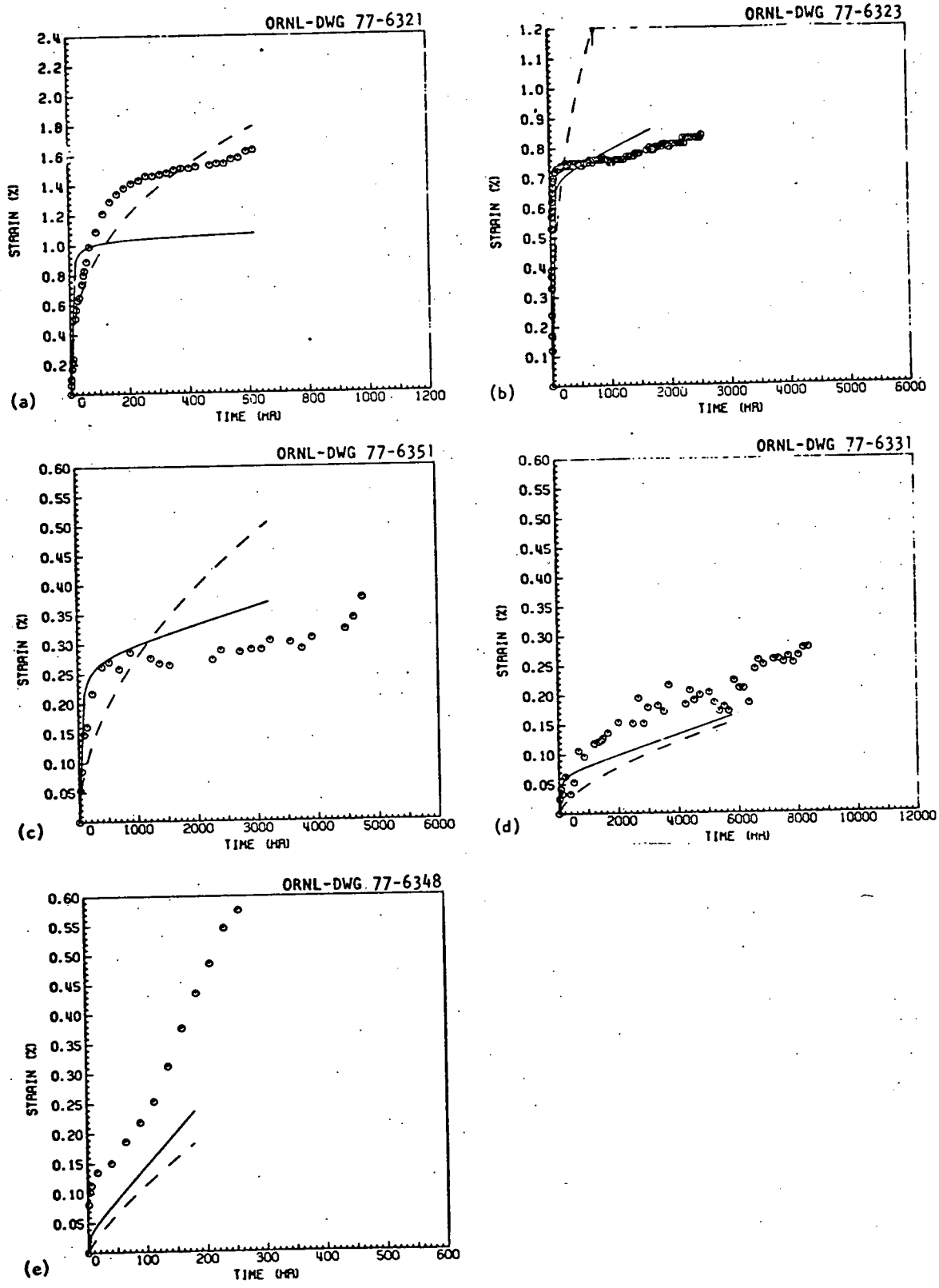

Fig. 18. Comparison of predicted creep strain-time behavior with experimental data. Solid lines predicted from the current equation. Dashed lines predicted from the Sterling equation. (a) Heat HH8735A, 345 MPa, 538°C; (b) Heat HH8735A, 207 MPa, 593°C; (c) Heat HH7686A, 103 MPa, 649°C; (d) Heat HH7686A, 55 MPa, 704°C; (e) Heat HH8808A, 55 MPa, 760°C.

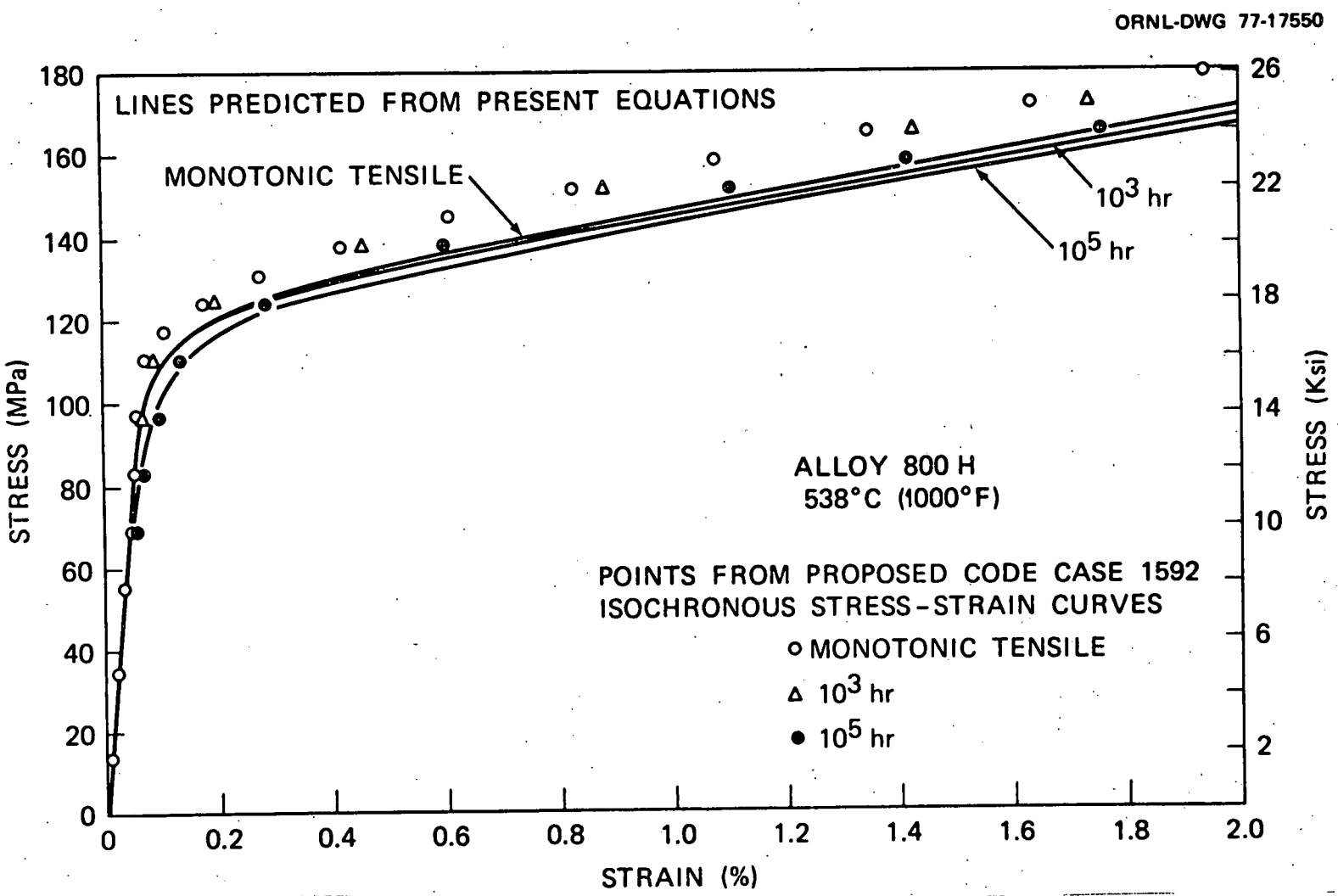

19. Comparison of isochronous stress-strain curves at 538°C (1000°F) predicted from the current equations with curves recently proposed for entry in Code Case 1592.

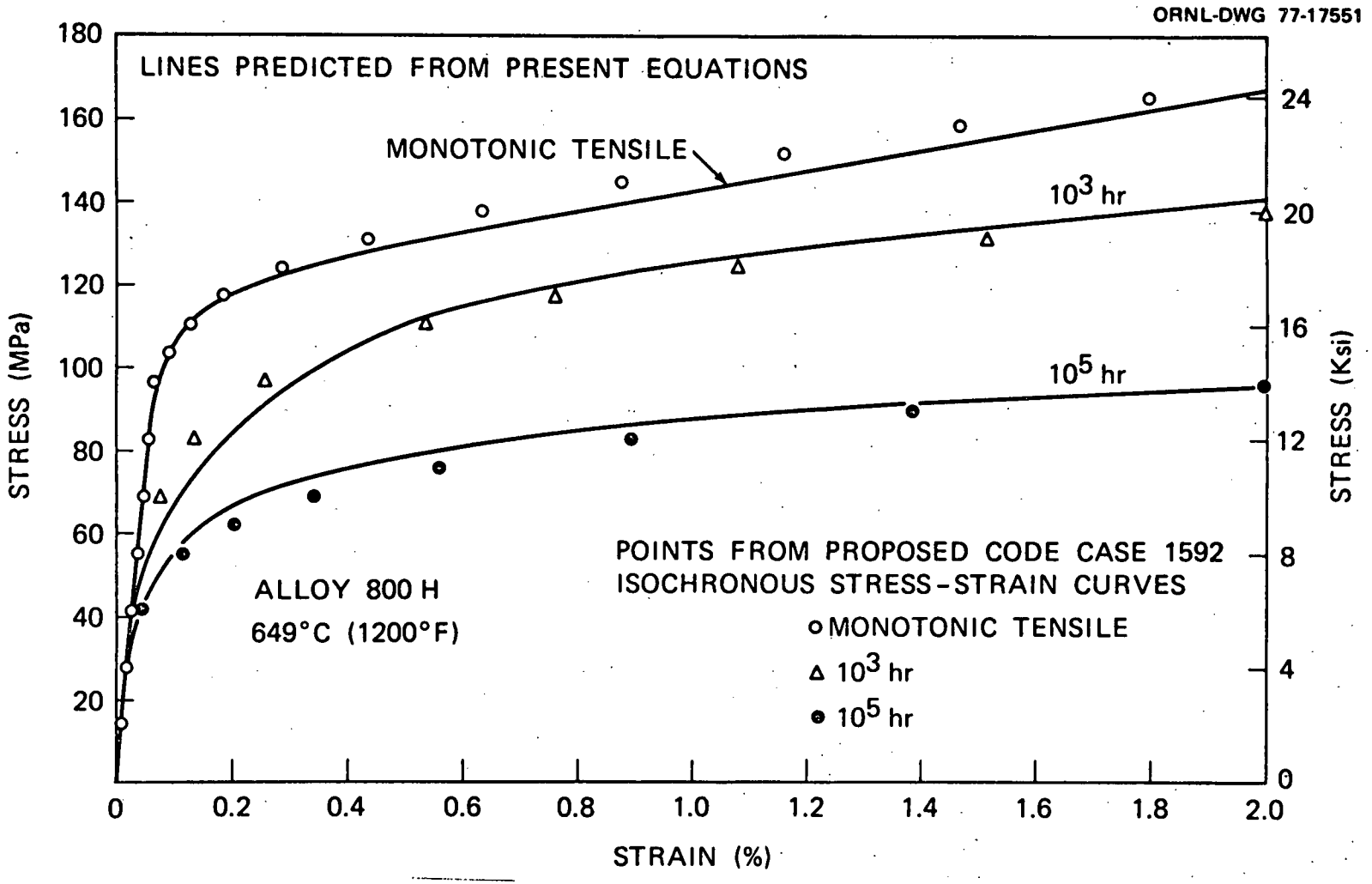

20. Comparison of isochronous stress-strain curves at 649°C (1200°F) predicted from the current equations with curves recently proposed for entry in Code Case 1592.

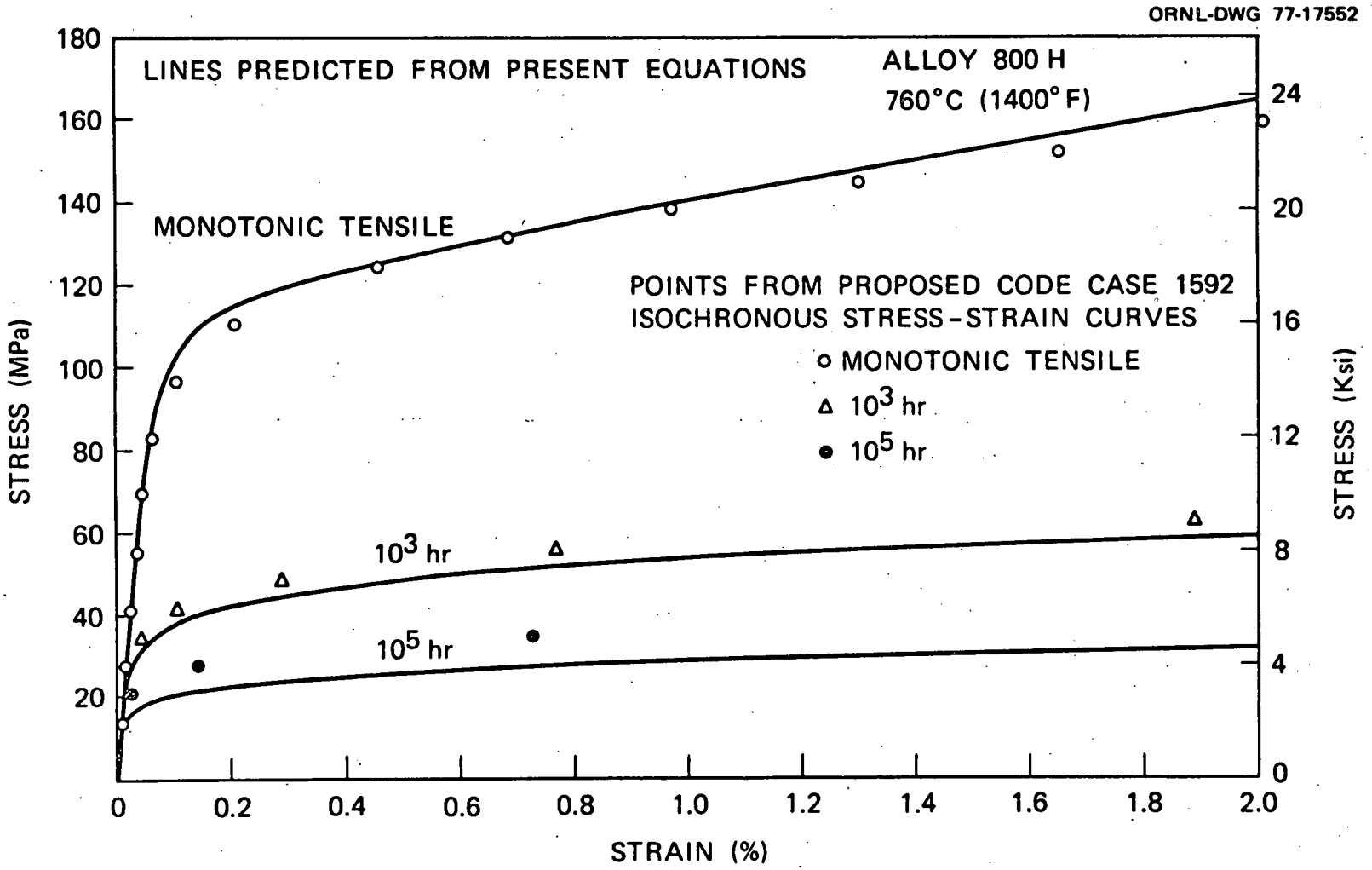

21. Comparison of isochronous stress-strain curves at 760°C (1400°F) predicted from the current equations with curves recently proposed for entry in Code Case 1592.